Control Design for a Non-Minimum Phase Hypersonic Vehicle Model

Thomas McKenna

A thesis submitted in partial fulfillment of the
requirements for the degree of

Master of Science

University of Washington

2016

Committee:

Anshu Narang-Siddarth

Mehran Mesbahi

Christopher Lum

Program Authorized to Offer Degree:
Aeronautics and Astronautics

©Copyright 2016
Thomas McKenna

University of Washington

Abstract

Control Design for a Non-Minimum Phase Hypersonic Vehicle Model

Thomas McKenna

Chair of the Supervisory Committee:
Assistant Professor Anshu Narang-Siddarth
Aeronautics and Astronautics

Air-breathing hypersonic vehicles are emerging as a method for cost-efficient access to space. Great strides have recently been made in the field of hypersonic vehicles, however the unique dynamics of the vehicles present challenges for control design. In this thesis, a nonlinear controller for a hypersonic vehicle model is designed using the Indirect Manifold Construction approach. The high fidelity hypersonic vehicle model considered in this thesis includes many of the challenging effects of hypersonic flight. The main challenge to control design is the vehicle's unstable internal dynamics. This non-minimum phase behavior prevents the use of many standard forms of nonlinear control techniques.

The nonlinear controller developed in this thesis following the Indirect Manifold Construction approach uses a hierarchical control design to force outputs to commanded values while ensuring the internal dynamics of the system remain stable. The nonlinear controller is shown to be effective in simulation. The closed loop system is also shown to be stable through a Lyapunov based stability analysis.

The views expressed are those of the author and do not reflect the official policy or position of the US Air Force, Department of Defense or the US Government.

TABLE OF CONTENTS

Page

List of Figures iii

List of Tables iv

Chapter 1: Introduction 1

Chapter 2: Vehicle Model 4
2.1 Truth Model 4
2.2 Control Design Model 7
2.3 CDM Validation 14

Chapter 3: Linear Optimal Control 17

Chapter 4: Control Design 22
4.1 Characterization of the Non-Minimum Phase System 22
4.2 Analysis of Zero Dynamics 24
4.3 Control Design using the Indirect Manifold Construction Approach 31
4.3.1 Step 1 32
4.3.2 Step 2 38
4.3.3 Step 3 38
4.3.4 Final Control Inputs 39
4.4 Simulation Results 39
4.5 Lyapunov Stability Analysis 44

Chapter 5: Conclusion 68

Bibliography 69

LIST OF FIGURES

Figure Number		Page
2.1	Geometry of the Hypersonic Vehicle.[1]	5
2.2	Cross Section of the Scramjet.[2]	6
2.3	C_L Curve-Fit over TM's Domain	11
2.4	C_T Curve-Fit over TM's Domain	11
2.5	Trim Conditions of the Truth Model	15
3.1	Pole-Zero Map of Closed Loop System.	21
4.1	Poles and Transmission Zeros of Linearized System.	24
4.2	Time Simulation with Zero Dynamics Control Inputs Applied.	31
4.3	Indirect Manifold Construction Approach.	32
4.4	Variation of Coefficient Driver Functions over Flight Envelope.	34
4.5	Variation of Coefficient Driver Functions over Flight Envelope.	35
4.6	Time Simulation of the Closed Loop System.	41
4.7	Time Simulation of the Closed Loop System.	42
4.8	Non-Minimum Phase Behavior of Flight Path Angle.	43
4.9	First Five Seconds of Time Simulation.	43
4.10	Bounding Function b_1.	46

LIST OF TABLES

Table Number Page

2.1 Range of Control Inputs. 7
2.2 Approximate Flight Envelope of the Truth Model. 7
2.3 Groupings of Curve-Fit Terms. 12
2.4 Average State Derivatives at Trim Conditions. 16
3.1 Trim Condition for Linearization. 18
4.1 Initial Condition for Zero Dynamics Simulation. 30
4.2 Initial Condition for Simulation. 40
4.3 Controller Gains used in Simulation. 40

ACKNOWLEDGMENTS

I would like to express my sincere gratitude to the University of Washington and the members of the Department of Aeronautics and Astronautics for giving me the opportunity to work alongside wonderful people, to take part in this challenging course of study, and to pursue this esteemed degree. My fellow students are among the finest people and most intelligent engineers I have had the pleasure of interacting with. I would like to thank Professor Anshu Narang-Siddarth, my Principle Investigator, for her constant guidance, patience, kindness, and willingness to "go through the math" with me one more time. Professor Narang-Siddarth is truly invested in the education and success of her students, and I will be forever grateful for the experience of working for her. I would like to thank Professor Mehran Mesbahi for his mentorship and apologize for the headaches I caused him in AA 510. I would like to thank Professor Christopher Lum for his time, friendliness, and interest in my work. I would like to thank the Professors of the Aeronautics and Astronautics and Applied Mathematics Departments whom I took classes and learned a lot from. I would like to thank the members of the Advanced Dynamics, Validation and Control Research Laboratory, especially Max, Armand, and Adam, for fielding my stupid questions and sharing laughs. I would like to thank Ed Connery and Leah Panganiban, Graduate Advising, for their support and consideration. Finally, I would like to thank my family and friends for their endless love and support.

Chapter 1
INTRODUCTION

Air-breathing hypersonic vehicles are emerging as a possible method for cost-efficient access to space. Interest in developing such a vehicle began in the 1960s. The United States government has made multiple attempts to develop an experimental proof of concept. In the 1990s, much of the developmental work for the X-30 (born out of the National Aero-Space Plane project) was completed although the program was canceled before a prototype was produced.[3] Following a failed test in 2001, NASA successfully flight tested the scramjet powered X-43A in 2004 and set a world speed record for a jet-powered aircraft at Mach 9.6 along the way.[4] Great strides have been made recently with the Boeing X-51 Waverider, a collaborative program managed by the US Air Force Research Laboratory. On its fourth flight in 2013, the X-51 performed its first fully successful flight test.[5] While the recent progress has been substantial, the unique dynamics of an air-breathing hypersonic vehicle present a challenging control problem that has not been completely explored.

There are many challenges associated with air-breathing hypersonic vehicles. These challenges include but are not limited to nonlinear dynamics, strong coupling between aerodynamic and propulsive effects, the high velocities and forces encountered at hypersonic speeds, and a flexible vehicle body. Creating a model of such a system also has unique challenges, such as modeling shock wave locations and scramjet performance. Pioneering work on the integration of Newtonian Dynamics, a scramjet propulsion system, and a flexible aircraft body into a mathematical model was done by Chavez and Schmidt in 1994.[6] The model considered in this thesis was originally developed by Bolender and Doman in 2005[7] and has been updated several times to include different effects and different control inputs.[1] It is

high-fidelity and captures many of the complicating effects stated earlier. The model includes longitudinal dynamics, a scramjet model, and a vibrational model. Oblique shock and Prandtl-Meyer theory are used to accurately calculate surface pressures that determine aerodynamic forces.

Several methods of control design for hypersonic vehicles are available in the literature. Early work was characterized by the use of linearized dynamics. The linear control methods presented are of varying complexities. Schmidt employed classic and multivariable linear control[8] for the model presented in his earlier work.[6] NASA performed flight control studies for its Hyper-X Research Vehicle using classical linear control design techniques including state feedback.[9] Setpoint tracking and regulator control were accomplished using Implicit Model Following[10] and a linearized version of Bolender and Doman's model.

There are also nonlinear control techniques proposed in the literature. An adaptive sliding mode controller was designed and analyzed for a generic hypersonic air vehicle.[11] An inversion-based design focused on robustness was synthesized for a generic hypersonic vehicle.[12] Neither of the generic hypersonic vehicle models considered in those studies offer the same level of complexity as the model used in this thesis. The generic hypersonic vehicle models do not consider the coupling that exists between elevator deflection and lift nor the coupling between the propulsion system and the pitching moment that exists due to the engine's location on the under side of the vehicle. The effects of the coupling that has been assumed insignificant by simpler models creates non-minimum phase behavior that may render the control designs used for simpler models unstable for the model used in this thesis.[2,13]

Fiorentini designed two adaptive nonlinear control systems for a slightly different variation of the TM developed by Bolender and Doman.[14] The first control system was designed for a version of the TM that uses three control inputs: fuel-to-air ratio, an elevator, and a canard. The canard was added to the TM to reduce the non-minimum phase behavior of the

system by effectively canceling the coupling between elevator deflection and lift. While the canard improves the controllability of the vehicle, it also adds complexity to the structure. This work focuses on a vehicle without the canard, leaving the fuel-to-air ratio and elevator as the only two control inputs. Fiorentini's second control system was also designed for a two control input model. However, it was designed using a simpler Control Design Model that does not include the effects of the flexible states and that assumes the coupling between the vehicle's elevator and drag is insignificant.

The largest challenge present in designing a controller for the given system is the system's exponentially unstable zero-dynamics. This non-minimum phase behavior prevents the use of many standard nonlinear control techniques, including dynamic inversion.

In this thesis, a nonlinear controller for a hypersonic vehicle is developed using the Indirect Manifold Construction approach developed by Narang-Siddarth and Valasek.[15] Chapter 2 contains a description of the hypersonic vehicle model, Chapter 3 contains an attempt at a linear controller, and Chapter 4 contains the derivation and analysis of the nonlinear controller. The hierarchical design of the nonlinear controller allows the closed-loop system to track desired outputs while ensuring stability of the system's internal dynamics. Simulation of the full nonlinear hypersonic vehicle model with the controller shows the controller's effectiveness. A Lyapunov based stability analysis also demonstrates the controller's validity.

Chapter 2
VEHICLE MODEL

Two distinct models of the longitudinal dynamics of a hypersonic vehicle are considered in this study. The Truth Model (TM) is a high fidelity model developed by Bolender and Doman.[1] A Control Design Model (CDM) of reduced-complexity was developed in this work and used in the control design. Controllers designed using the CDM are validated through closed-loop simulation of the TM.

2.1 Truth Model

The TM assumes the geometry shown in Figure 2.1 for the hypersonic vehicle. Hypersonic vehicles are generally assumed to be flexible due to their material construction and shape. For the vibrational model of the fuselage, Bolender and Doman consider a two cantilever beam structure that is clamped at the center of mass.[2] The dynamic simulation considers only the vehicle's transverse vibration that is forced by the aerodynamic forces acting on the cantilever beams. Oblique shock and Prandtl-Meyer theory are applied to calculate surface pressures on the vehicle.

To achieve the velocity needed for hypersonic flight, hypersonic vehicles are typically designed to use rocket propulsion or supersonic combustion ramjet engines (scramjets). The hypersonic vehicle in this study has a scramjet on its underside. A cross section of the scramjet is shown in Figure 2.2. The thrust produced by the scramjet is calculated using a model developed by Chavez and Schmidt.[6] The two variables that control thrust production in scramjets are heat addition in the combustion chamber and diffuser area ratio. The heat addition changes based on throttle setting and the diffuser area ratio is a design feature.

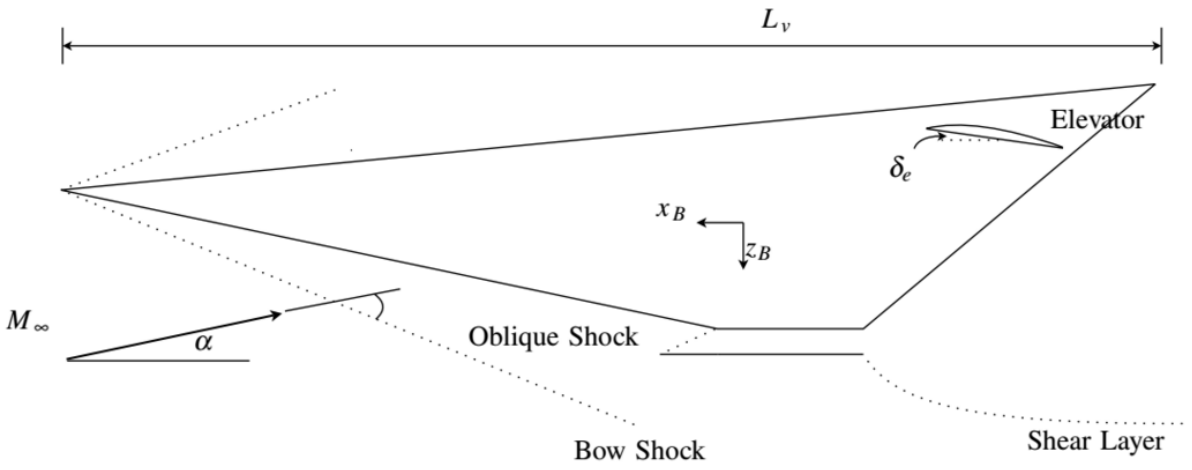

Figure 2.1: Geometry of the Hypersonic Vehicle.[1]

The thrust produced depends heavily on the mass flow through the engine. The nose of the vehicle creates an oblique shock wave at hypersonic speeds. The mass flow through the engine is a function of the angle of that shock wave, along with the vehicle's angle of attack and Mach number. Many models of hypersonic vehicles assume that the bow shock stays nearly attached as the flight envelopes of these vehicles are encompassed of high Mach numbers. The TM does not make this assumption. If the bow shock angle becomes too great at the vehicles lower Mach numbers it can cause "mass flow spillage" by forcing air outside of the inlet. The inlet has a cow lip on the bottom. In order to maximize mass flow through the engine and therefore performance, the hypersonic vehicle in the TM has been designed with a translating cow lip. The cowl lip is assumed to change length instantaneously to be exactly coincident with the bow shock. While this variable length does increase engine performance, it also adds computational complexity to the TM as the aerodynamic forces acting on the vehicle are effected by a change in cowl door length.

The longitudinal dynamics for a flexible aircraft are derived using Lagrange's Equations. The coupling between the rigid body and flexible dynamics occurs through the aerodynamic

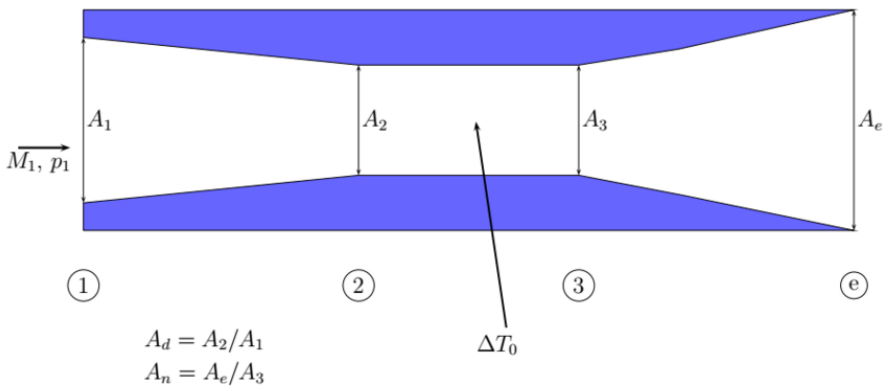

Figure 2.2: Cross Section of the Scramjet.[2]

forces acting on the vehicle. The equations of motion for the vehicle are given below.

$$\dot{V} = \frac{T cos\alpha - D}{m} - g sin(\theta - \alpha) \tag{2.1}$$

$$\dot{\alpha} = \frac{-T sin\alpha - L}{mV} + Q + \left(\frac{g}{V} - \frac{V}{r}\right) cos(\theta - \alpha) \tag{2.2}$$

$$\dot{Q} = \frac{M_y}{I_{yy}} \tag{2.3}$$

$$\dot{h} = V sin(\theta - \alpha) \tag{2.4}$$

$$\dot{\theta} = Q \tag{2.5}$$

$$\ddot{\eta}_i = -2\zeta_i\omega_i\dot{\eta}_i - \omega_i^2\eta_i + N_i, \qquad i = 1, 2, 3 \tag{2.6}$$

This model is comprised of five rigid body state variables $x = [V, \alpha, Q, h, \theta]^T$, six flexible states $\eta = [\eta_1, \dot{\eta}_1, \eta_2, \dot{\eta}_2, \eta_3, \dot{\eta}_3]^T$, and two control inputs $u = [\delta_e, \phi]^T$. The elevator deflection δ_e effects the lift and drag forces in the equations of motion, creating non-minimum phase behavior. The fuel-to-air ratio ϕ is essentially a measure of throttle and effects the thrust. Any change in thrust also effects the vehicle's pitching moment and lift as the engine is

located on the underside of the vehicle. The vehicle's range of control inputs is shown in Table 2.1.

Table 2.1: Range of Control Inputs.

Control Input	Lower Bound	Upper Bound
δ_e (deg)	-15	15
ϕ	0.1	1.1

The TM is approximately valid over the flight envelope shown in Table 2.2. There are specific cases within the specified flight envelope where the TM will break down if flight conditions violate assumptions made in the derivation of the model (such as formation of unexpected shock waves or a large decrease in mass flow through the engine).

Table 2.2: Approximate Flight Envelope of the Truth Model.

Parameter	Lower Bound	Upper Bound
M	8	12
h (ft)	85,000	135,000
α (deg)	-5	10

The TM is coded in MATLAB.

2.2 Control Design Model

This CDM has been derived to allow for control design and stability analysis. The approach used in this derivation follows the approach taken by Parker *et al* and Fiorentini.[13,14] The approach consists of replacing the aerodynamic and propulsive forces and pitching moment

with curve-fitted functions of the rigid-body states, the flexible states, and the control inputs. This approximation retains the most critical behaviors of the TM.

In order to simplify analysis, the equations of motion can be re-scaled for the CDM by replacing the velocity state with Mach number and speed of sound.

$$\dot{M} = \frac{T cos\alpha - D}{m v_s} - \frac{g}{v_s} sin(\theta - \alpha) \tag{2.7}$$

$$\dot{\alpha} = \frac{-T sin\alpha - L}{m M v_s} + Q + \left(\frac{g}{M v_s} - \frac{M v_s}{r} \right) cos(\theta - \alpha) \tag{2.8}$$

$$\dot{Q} = \frac{M_y}{I_{yy}} \tag{2.9}$$

$$\dot{h} = M v_s sin(\theta - \alpha) \tag{2.10}$$

$$\dot{\theta} = Q \tag{2.11}$$

With the equations of motion stated in this manner, Mach number tracking is more straightforward.

The aerodynamic and propulsive forces and pitching moment in the CDM are approximated by expressions including dynamic pressure and force/moment coefficients.

$$L \approx \frac{1}{2} \rho V^2 S C_L(\alpha, \delta_e, \eta_i) \tag{2.12}$$

$$D \approx \frac{1}{2} \rho V^2 S C_D(\alpha, \delta_e, \eta_i) \tag{2.13}$$

$$T \approx \frac{1}{2} \rho V^2 S C_T(\alpha, \phi, \eta_i) \tag{2.14}$$

$$M_y \approx z_T T(\alpha, \phi, \eta_i, V) + \frac{1}{2} \rho V^2 S \bar{c} C_M(\alpha, \delta_e, \eta_i) \tag{2.15}$$

The coefficients of lift and drag (C_L, C_D) in these approximations are functions of angle of attack, elevator deflection, and the flexible states. The coefficient of thrust C_T is a function of angle of attack, fuel-to-air ratio, and the flexible states. The coefficient of the pitching

moment C_M is a function of angle of attack, the flexible states, and elevator deflection. It is easy to see the additional contribution to the pitching moment created by the thrust vector in the expression for M_y above, where the z_T term is a constant related to the engine's location on the underside of the vehicle.

Substituting the approximations for the aerodynamic and propulsive forces and pitching moments into the re-scaled equations of motion gives the following equations of motion for the CDM.

$$\dot{M} = \frac{\left(\frac{1}{2}\rho(Mv_s)^2 SC_T\right) cos\alpha - \left(\frac{1}{2}\rho(Mv_s)^2 SC_D\right)}{mv_s} - \frac{g}{v_s} sin(\theta - \alpha) \tag{2.16}$$

$$\dot{\alpha} = \frac{-\left(\frac{1}{2}\rho(Mv_s)^2 SC_T\right) sin\alpha - \left(\frac{1}{2}\rho(Mv_s)^2 SC_L\right)}{mMv_s} + Q + \left(\frac{g}{Mv_s} - \frac{Mv_s}{r}\right) cos(\theta - \alpha) \tag{2.17}$$

$$\dot{Q} = \frac{\left(z_T\left(\frac{1}{2}\rho V^2 SC_T(\alpha, \phi, \eta_i)\right) + \frac{1}{2}\rho(Mv_s)^2 S\bar{c}C_M\right)}{I_{yy}} \tag{2.18}$$

$$\dot{h} = Mv_s sin(\theta - \alpha) \tag{2.19}$$

$$\dot{\theta} = Q \tag{2.20}$$

The force and moment coefficients that appear in the approximations above were found using a curve-fitting technique that encompasses the entire flight envelope of the hypersonic vehicle. The curve-fits for the coefficients are shown below.

$$C_L = C_L^{\alpha}\alpha + C_L^{\delta_e}\delta_e + C_L^0 + C_L^{\eta_1}\eta_1 + C_L^{\eta_2}\eta_2 + C_L^{\eta_3}\eta_3 \tag{2.21}$$

$$C_D = C_D^{\alpha^2}\alpha^2 + C_D^{\alpha}\alpha + C_D^{\delta_e^2}\delta_e^2 + C_D^{\delta_e}\delta_e + C_D^0 + C_D^{\eta_1}\eta_1 + C_D^{\eta_2}\eta_2 + C_D^{\eta_3}\eta_3 \tag{2.22}$$

$$C_M = C_M^{\alpha^2}\alpha^2 + C_M^{\alpha}\alpha + C_M^{\delta_e}\delta_e + C_M^0 + C_M^{\eta_1}\eta_1 + C_M^{\eta_2}\eta_2 + C_M^{\eta_3}\eta_3 \tag{2.23}$$

$$C_T = C_T^{\alpha^3\phi}\alpha^3\phi + C_T^{\alpha^2\phi}\alpha^2\phi + C_T^{\alpha\phi}\alpha\phi + C_T^{\phi}\phi + C_T^{\alpha^3}\alpha^3 + C_T^{\alpha^2}\alpha^2 + C_T^{\alpha}\alpha + C_T^0 + \sum_{i=1}^{3} C_T^{\eta_i}\eta_i \tag{2.24}$$

Plots of two of the curve-fits are shown in Figures 2.3 and 2.4. The plot of the curve-fit for C_L shows the value of C_L as it varies with δ_E and α. While Figure 2.3 shows the variation with δ_E and α, the value of C_L also varies with changes in altitude and velocity. The actual values of C_L are denoted by the black dots. The x's above and below the dots indicate the maximum and minimum values of C_L calculated for the TM domain. These x's are meant to show how C_L varies with changes in other parameters. For example, the maximum C_L is most likely occurring at the TM's lowest altitude. As Figure 2.3 shows, most of the variation in C_L occurs with δ_E and α.

Examining the plot of the curve-fit for C_T yields a slightly different result. Figure 2.4 shows the value of C_T as it varies with ϕ and α. Once again, the value of C_T also varies with changes in altitude and velocity. These variations, shown by the maximum and minimum values of C_T marked with x's, can be quite large. It makes sense for the variation of C_T to be larger than that of C_L as the amount of thrust that a scramjet produces is much more sensitive to changes in altitude and velocity than the amount of lift that a body produces. These larger variations are accounted for with more terms in the curve-fit.

To better study the direct effects of the two control inputs on the dynamics of the vehicle, the curve-fits for the aerodynamic and propulsive coefficients can be separated into different pieces. The pieces are chosen such that terms directly dependent on either of the control inputs are separated from the terms that do not directly depend on the control inputs. The short-hand definitions listed in Table 2.3 are used to simplify the terms from the curve-fits for use in this thesis.

Substituting the definitions given in Table 2.3 into the equations of motion gives the following equations.

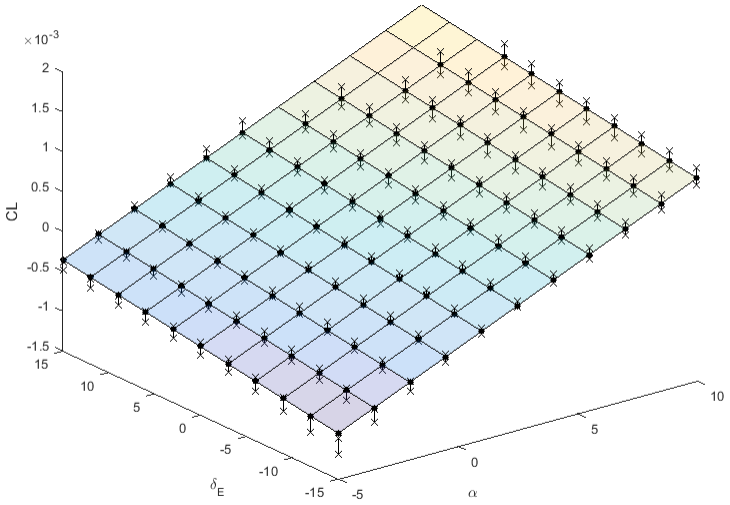

Figure 2.3: C_L Curve-Fit over TM's Domain

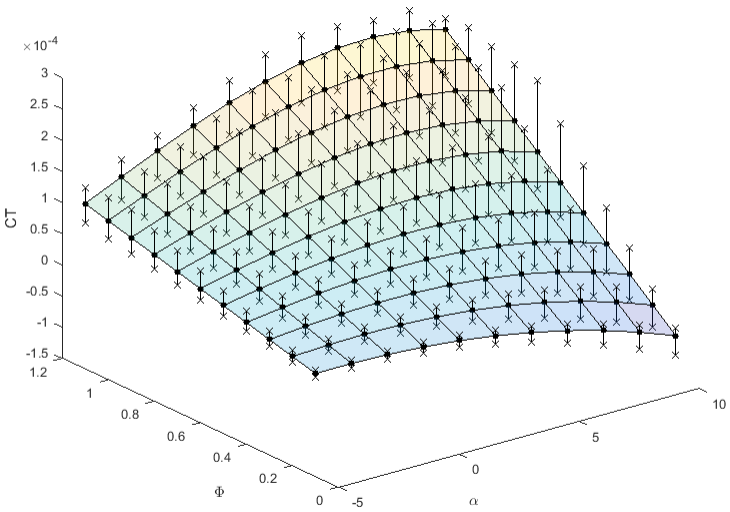

Figure 2.4: C_T Curve-Fit over TM's Domain

Table 2.3: Groupings of Curve-Fit Terms.

Definition	Curve-Fit Terms
l_0	$C_L^0 + C_L^\alpha \alpha + C_L^{\eta_1}\eta_1 + C_L^{\eta_2}\eta_2 + C_L^{\eta_3}\eta_3$
l_1	$C_L^{\delta_e}$
d_0	$C_D^0 + C_D^{\alpha^2}\alpha^2 + C_D^\alpha \alpha + C_D^{\eta_1}\eta_1 + C_D^{\eta_2}\eta_2 + C_D^{\eta_3}\eta_3$
d_1	$C_D^{\delta_e}$
d_2	$C_D^{\delta_e^2}$
m_0	$C_M^0 + C_M^{\alpha^2}\alpha^2 + C_M^\alpha \alpha + C_M^{\eta_1}\eta_1 + C_M^{\eta_2}\eta_2 + C_M^{\eta_3}\eta_3$
m_1	$C_M^{\delta_e}$
t_0	$C_T^0 + C_T^{\alpha^3}\alpha^3 + C_T^{\alpha^2}\alpha^2 + C_T^\alpha \alpha + C_T^{\eta_1}\eta_1 + C_T^{\eta_2}\eta_2 + C_T^{\eta_3}\eta_3$
t_1	$C_T^{\alpha^3\phi}\alpha^3 + C_T^{\alpha^2\phi}\alpha^2 + C_T^{\alpha\phi}\alpha + C_T^\phi$

$$\dot{M} = \frac{(\frac{1}{2}\rho(Mv_s)^2 S)((t_0 + t_1\phi)cos\alpha - (d_0 + d_1\delta_e + d_2\delta_e^2))}{mv_s} - \frac{g}{v_s} sin(\theta - \alpha) \tag{2.25}$$

$$\dot{\alpha} = \frac{-(\frac{1}{2}\rho(Mv_s)^2 S)((t_0 + t_1\phi)sin\alpha - (l_0 + l_1\delta_e))}{mMv_s} + Q + \left(\frac{g}{Mv_s} - \frac{Mv_s}{r}\right) cos(\theta - \alpha) \tag{2.26}$$

$$\dot{Q} = \frac{(\frac{1}{2}\rho(Mv_s)^2 S)(z_T(t_0 + t_1\phi) + \bar{c}(m_0 + m_1\delta_e))}{I_{yy}} \tag{2.27}$$

$$\dot{h} = Mv_s sin(\theta - \alpha) \tag{2.28}$$

$$\dot{\theta} = Q \tag{2.29}$$

Note that the individual control inputs are now directly present in the equations of motion. For further simplification, the following variables are introduced.

$$c_0 = \frac{\rho M^2 v_s S}{2m}(t_0 cos\alpha - d_0) = \frac{\bar{q}S}{mv_s}(t_0 cos\alpha - d_0) \tag{2.30}$$

$$c_1 = \frac{\rho M^2 v_s S}{2m} t_1 = \frac{\bar{q}S}{mv_s} t_1 \tag{2.31}$$

$$c_2 = \frac{\rho M^2 v_s S}{2m} d_1 = \frac{\bar{q}S}{mv_s} d_1 \tag{2.32}$$

$$c_3 = \frac{\rho M^2 v_s S}{2m} d_2 = \frac{\bar{q}S}{mv_s} d_2 \tag{2.33}$$

$$c_4 = \frac{g}{v_s} \tag{2.34}$$

$$c_5 = \frac{\rho M v_s S}{2m}(t_0 sin\alpha - l_0) = \frac{\bar{q}S}{mMv_s}(t_0 sin\alpha - l_0) \tag{2.35}$$

$$c_6 = \frac{\rho M v_s S}{2m} l_1 = \frac{\bar{q}S}{mMv_s} l_1 \tag{2.36}$$

$$c_7 = \frac{v_s}{r} \tag{2.37}$$

$$c_8 = \frac{\rho M^2 v_s^2 S}{2I_{yy}}(z_T t_0 + \bar{c} m_0) = \frac{\bar{q}S}{I_{yy}}(z_T t_0 + \bar{c} m_0) \tag{2.38}$$

$$c_9 = \frac{\rho M^2 v_s^2 S}{2I_{yy}} z_T t_1 = \frac{\bar{q}S}{I_{yy}} z_T t_1 \tag{2.39}$$

$$c_{10} = \frac{\rho M^2 v_s^2 S}{2I_{yy}} \bar{c} m_1 = \frac{\bar{q}S}{I_{yy}} \bar{c} m_1 \tag{2.40}$$

The variables allow the CDM's equations of motion to be arranged into a compact form. Of these variables; c_4 and c_7 are constant; c_0, c_1, c_8, and c_9 are functions of Mach number and angle of attack; c_5 is a function of angle of attack; and c_2, c_3, c_6, and c_{10} are functions of Mach number. Many of the variables are also functions of the flexible states, but for simplicity the notation of the flexible states has been omitted in the compact form of the CDM's equations of motion. The compact form of the CDM's equations of motion is shown below.

$$\dot{M} = c_0(\alpha, M) + c_1(\alpha, M)\phi cos\alpha + c_2(M)\delta_e + c_3(M)\delta_e^2 - c_4 sin(\theta - \alpha) \tag{2.41}$$

$$\dot{\alpha} = -c_5(\alpha) - \frac{c_1(\alpha, M)}{M}\phi sin\alpha + c_6(M)\delta_e + Q + \frac{c_4}{M}cos(\theta - \alpha) - c_7 M cos(\theta - \alpha) \tag{2.42}$$

$$\dot{Q} = c_8(\alpha, M) + c_9(\alpha, M)\phi + c_{10}(M)\delta_e \tag{2.43}$$

$$\dot{h} = M v_s sin(\theta - \alpha) \tag{2.44}$$

$$\dot{\theta} = Q \tag{2.45}$$

2.3 CDM Validation

In order to validate the behavior of the CDM, the behavior of the CDM was compared to the behavior of the TM at several trim conditions. The TM finds trim conditions by using the 'fmincon' MATLAB function to minimize the state derivative vector $\dot{x}$ subject to certain constraints and tolerances. For this validation exercise, a total of 99 sample trim conditions that span the TM's flight envelope were found. Figure 2.5 shows the sample trim conditions for the TM. Note that there are the same number of trim conditions at each Mach number. The trim conditions at the higher Mach numbers are slightly harder to see as they group around angles of attack near zero. These low angles of attack are expected at such high velocities.

As the TM is very complex, the tolerances used when executing the 'fmincon' function do allow some of the state derivatives to have nonzero values. This enables the function to find a solution in reasonable time. The fact that the solutions found for trimmed states are not exact does not hinder our control design process in any way.

The state derivatives of both the TM and the CDM at each of the 99 trim conditions were calculated. A comparison of the average of the state derivatives across all 99 specific cases is shown in Table 2.4.

The state derivatives of the CDM compare reasonably to the state derivatives of the

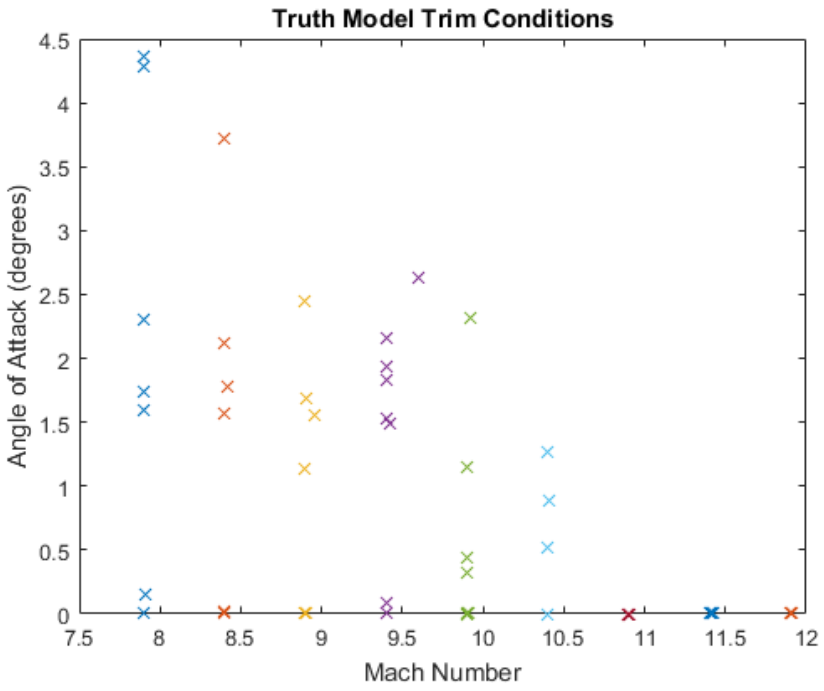

Figure 2.5: Trim Conditions of the Truth Model

TM. Both have small values for $\dot{V}$ and $\dot{\alpha}$. The difference in $\dot{Q}$ is reasonable considering the imperfect trim conditions. Therefore the CDM is valid over the sampling of trim conditions that span the TM's flight envelope.

Table 2.4: Average State Derivatives at Trim Conditions.

State Derivative	TM	CDM
$\dot{V}$ (ft/s^2)	-1.2806	-4.4741
$\dot{\alpha}$ (deg/s)	0.0688	0.0745
$\dot{Q}$ (deg/s^2)	3.4779	-2.7215
$\dot{h}$ (ft/s)	0	0
$\dot{\theta}$ (deg/s)	0	0

Chapter 3

LINEAR OPTIMAL CONTROL

In the literature, there are several examples of linear controllers designed for linearized versions of hypersonic vehicle models. An attempt at designing a linear optimal controller was made in this thesis to have a baseline controller of the linearized system which could then be tested in the nonlinear system and compared to the nonlinear controller design. In this chapter, the attempt at designing an optimal control design for a linearized version of the TM is explained and the controller ultimately is unsuccessful. The control design follows the approach taken by Groves et al.[10] for a 2005 version of Bolender and Doman's model. That model included a canard and therefore a third control input. The TM used in this thesis only includes two control inputs. The challenges presented by this reduced control authority are discussed in the preceding chapter.

In this chapter, only the rigid body plant dynamics are considered. This exclusion of the flexible states simplifies the control design. The linearized plant can be described by the following state space equations.

$$\dot{x}_p = A_p x_p + B_p u_p \tag{3.1}$$

$$y_p = C_p x_p \tag{3.2}$$

$$z_p = H_p x_p \tag{3.3}$$

In this plant, $x_p \in \mathbb{R}^5$ is the $5x1$ state vector, $u_p \in \mathbb{R}^2$ is the $2x1$ control input, $y_p \in \mathbb{R}^9$ is the $5x1$ output available for feedback, and $z_p = (V_t \;\; \alpha)^T$ is the $2x1$ performance output to be regulated to a desired reference command. The results of the linearization produce the

following plant dynamics.

$$A_p = \begin{pmatrix} X_v & X_a & 0 & X_h & -g \\ \frac{Z_v}{V_0} & \frac{Z_\alpha}{V_0} & \frac{1-Z_q}{V_0} & \frac{Z_h}{V_0} & 0 \\ M_v & M_\alpha & M_q & M_h & 0 \\ 0 & -V_0 & 0 & 0 & V_0 \\ 0 & 0 & 1 & 0 & 0 \end{pmatrix} \tag{3.4}$$

$$B_p = \begin{pmatrix} X_{\delta_e} & X_{\delta_\phi} \\ \frac{Z_{\delta_e}}{V_0} & \frac{Z_{\delta_\phi}}{V_0} \\ M_{\delta_e} & M_{\delta_\phi} \\ 0 & 0 \\ 0 & 0 \end{pmatrix} \tag{3.5}$$

The exact expressions for each of the dimensional stability derivatives present in the dynamics above are given by Bolender and Doman.[2] In this case, the dynamics were linearized about the trim condition given in Table 3.1.

Table 3.1: Trim Condition for Linearization.

State	Trim Value
M_0	8.89
α_0	2.0397 deg
γ_0	0 deg
Q_0	0 deg/s
h_0	104007 ft

For added model accuracy, a simple model of actuator dynamics was added to the plant

dynamics. The actuator dynamics are modeled as follows.

$$x_\delta = A_\delta x_\delta + B u_\delta \tag{3.6}$$

$$A_\delta = \begin{pmatrix} -20 & 0 \\ 0 & -10 \end{pmatrix}, \quad B_\delta = \begin{pmatrix} 20 & 0 \\ 0 & 10 \end{pmatrix} \tag{3.7}$$

$$x_\delta = \begin{pmatrix} x_{\delta_e} \\ x_\phi \end{pmatrix}, \quad u_\delta = \begin{pmatrix} u_{\delta_e} \\ u_\phi \end{pmatrix} \tag{3.8}$$

These actuator dynamics were used by Groves et al.[10] and were chosen to approximate values for real actuators. The actuator dynamics are appended to the plant dynamics as shown below.

$$\dot{x}_1 = A_1 x_1 + B_1 u_1 \tag{3.9}$$

$$y_1 = C_1 x_1 \tag{3.10}$$

$$z_1 = H_1 x_1 \tag{3.11}$$

$$A_1 = \begin{pmatrix} A_p & B_p \\ 0 & A_\delta \end{pmatrix}, \quad B_1 = \begin{pmatrix} 0 \\ B_\delta \end{pmatrix}, \quad H_1 = \begin{pmatrix} H_p & 0 \end{pmatrix} \tag{3.12}$$

Groves et al. developed two controllers using this new linearized model.[10] Both designs used LQ optimization techniques, and specifically the Linear Quadratic Regulator (LQR) algorithm for gain scheduling. The two designs differ in how they attempt to eliminate steady state feedback error. The strengths and weaknesses of the two different controllers are not as important in the context of this thesis. Only the second control design strategy was attempted as part of this thesis.

The second approach to designing a linear controller was to transform the tracking problem into a regulation problem and then use LQR optimization techniques. Groves et al.

describe the tracking error with the following dynamics.

$$\dot{x}_1 = A_1 x_1 + B_1 u_p \tag{3.13}$$

$$e_1 = H_1 x_1 \tag{3.14}$$

To integrate the error into the system, the additional dynamics $\dot{x}_2 = -e_1$ are defined and then appended to the system in the following manner.

$$\begin{pmatrix} \dot{x}_1 \\ \dot{x}_2 \end{pmatrix} = \begin{pmatrix} A_1 & 0 \\ -H_1 & 0 \end{pmatrix} \begin{pmatrix} x_1 \\ x_2 \end{pmatrix} + \begin{pmatrix} B_1 \\ 0 \end{pmatrix} u_p. \tag{3.15}$$

The equation above can be written in the standard form as shown below.

$$\begin{aligned} \dot{\bar{x}} &= A\bar{x} + Bu_p \\ e &= -H\bar{x}. \end{aligned} \tag{3.16}$$

Instead of a tracking problem, the problem posed above is a standard regulator problem.

LQR gain scheduling is used to find an optimal control. The following is a standard cost function definition.[16]

$$J = \frac{1}{2}\int_0^\infty (e^T Q e + u^T R u) dt \tag{3.17}$$

The $e^T Q e$ portion of the cost function represents the total output error and the $u^T R u$ portion of the function represents the input energy into the system. Q and R are matrices that are used to appropriately "weigh" the importance of output error against input energy. A larger Q penalizes output error more harshly while a larger R penalizes input energy more harshly. Selecting these matrices such that our cost function can be optimized requires $Q = Q^T \geq 0, R = R^T > 0$. The positive semi-definiteness and semi-definiteness of the Q and R matrices ensure that J is well defined.

Attempts at getting a linear optimal controller to drive the current two control input hypersonic vehicle model to commanded states were unsuccessful in this thesis. The poles of the closed loop system are shown in Figure 3.1.

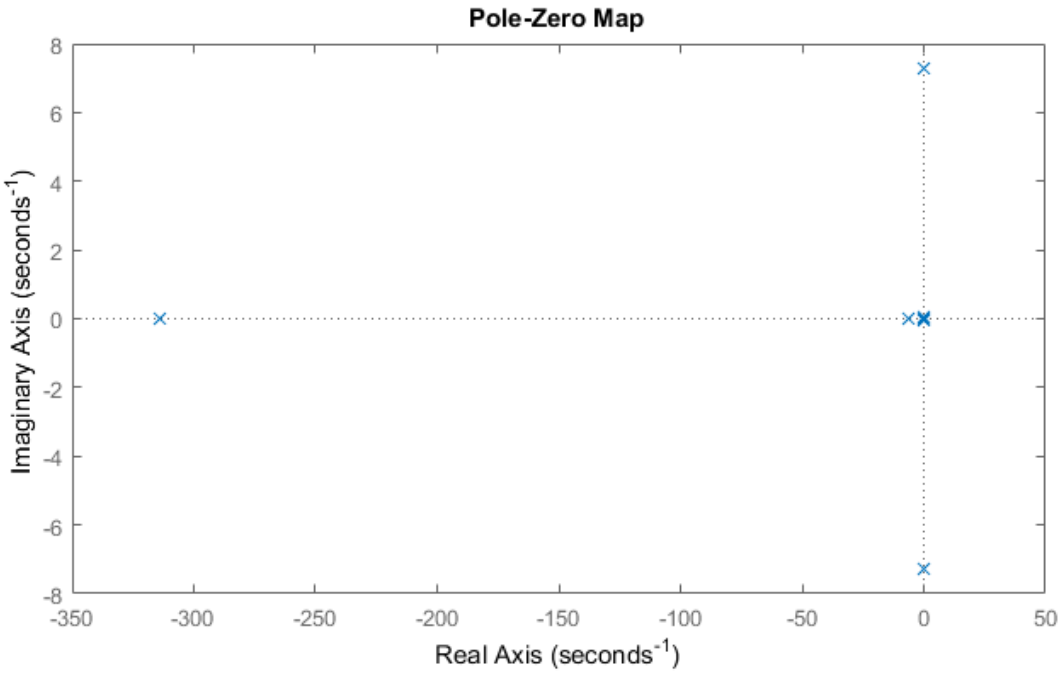

Figure 3.1: Pole-Zero Map of Closed Loop System.

The initial change in pitch was never recovered from in any simulations of a closed loop system with a linear optimal controller. The hypersonic vehicle rapidly loses control as the pitch angle increases dramatically.

Chapter 4

CONTROL DESIGN

The design of a robust, nonlinear controller is accomplished using the Indirect Manifold Construction approach developed by Narang-Siddarth and Valasek.[15] This hierarchical design approach for the control of nonlinear, nonstandard forms of singularly perturbed systems can be applied to control non-minimum phase systems. The Indirect Manifold Construction approach has been successfully used to control missiles that display non-minimum phase behavior[17] similar to the hypersonic vehicle being considered in this thesis. The approach drives outputs to desired values while ensuring any unstable internal dynamics approach zero over time. This chapter includes a characterization of the hypersonic vehicle model as a non-minimum phase system, an analysis of the system's zero dynamics, the derivation of the stabilizing control law, simulation results showing the control law's effectiveness, and Lyapunov stability analysis.

4.1 Characterization of the Non-Minimum Phase System

"Non-Minimum Phase" is used to describe the class of systems governed by unstable internal dynamics. "Internal dynamics" are the dynamics of the states not included in the control design.[15] For example, one may linearize the system of equations that govern the hypersonic vehicle model about a trim condition. The altitude dynamics can be ignored as they do not

effect any of the system's other states. This linearized system is of the following form.

$$\dot{x} = \begin{bmatrix} \dot{M} \\ \dot{\gamma} \\ \dot{Q} \\ \dot{\alpha} \end{bmatrix} = [A]_{4x4} \begin{bmatrix} M \\ \gamma \\ Q \\ \alpha \end{bmatrix} + [B]_{4x2} \begin{bmatrix} \delta_e \\ \phi \end{bmatrix} \tag{4.1}$$

$$y = \begin{bmatrix} M \\ \gamma \end{bmatrix} \tag{4.2}$$

This system has four states and two outputs. If an output feedback controller is introduced to drive the two outputs to desired reference conditions M_r and γ_r, two states remain that are effectively uncontrolled (Q and α). The dynamics of these two states that are not considered in the control design are called the system's "internal dynamics." While some systems have stable internal dynamics, a particular challenge is offered by the non-minimum phase systems that have unstable internal dynamics.

Linearizing the system of equations that govern the TM about a trim condition allows an inspection of the poles and transmission zeros of the open loop system. Slotine and Li showed that a zero in the right half-plane of a linearized system is a necessary and sufficient condition for the nonlinear system to be non-minimum phase.[18] The system was linearized about the trim condition given in Table 3.1. The poles and transmission zeros of the linearized open loop TM are shown in Figure 4.1 as X's and O's. The three complex conjugate pairs of poles and zeros correspond to the flexible modes. These modes are shown to be oscillatory with a very high frequency, but stable. This is important because in the design of the controller, the flexible states are not explicitly controlled (they are internal states). However, because the dynamics of these internal states are stable, they are considered as small perturbations in the control design and do not have to be explicitly controlled. The poles and zeros located very close to the origin indicate a slightly unstable phugoid mode. The poles and zeros that

appear to be mirror images of each other across the y-axis correspond to pitch and altitude modes. The pitch mode accounts for the zero in the far right half plane and thus the non-minimum phase behavior. In summary, the linearized dynamics of the hypersonic vehicle model include two transmission zeros in the right half plane, indicating that the nonlinear system is non-minimum phase.

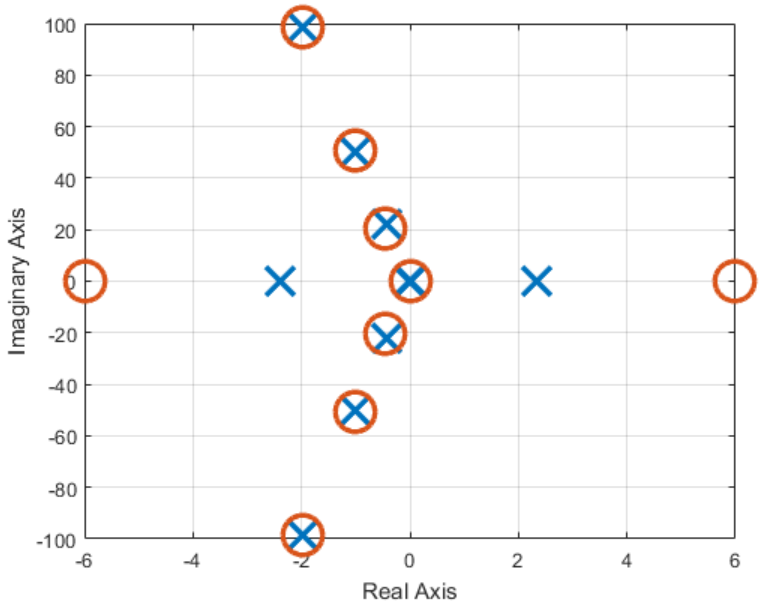

Figure 4.1: Poles and Transmission Zeros of Linearized System.

4.2 Analysis of Zero Dynamics

An analysis of the zero dynamics of this system may help determine the feasibility of a standard nonlinear state feedback controller. In Chapter 2, the compact form of the nonlinear

equations of motion of the CDM was given as follows.

$$\dot{M} = c_0(\alpha, M) + c_1(\alpha, M)\phi cos\alpha + c_2(M)\delta_e + c_3(M)\delta_e^2 - c_4 sin(\theta - \alpha) \tag{4.3}$$

$$\dot{\alpha} = -c_5(\alpha) - \frac{c_1(\alpha, M)}{M}\phi sin\alpha + c_6(M)\delta_e + Q + \frac{c_4}{M}cos(\theta - \alpha) - c_7 M cos(\theta - \alpha) \tag{4.4}$$

$$\dot{Q} = c_8(\alpha, M) + c_9(\alpha, M)\phi + c_{10}(M)\delta_e \tag{4.5}$$

$$\dot{h} = M v_s sin(\theta - \alpha) \tag{4.6}$$

$$\dot{\theta} = Q \tag{4.7}$$

The control objective is to regulate the Mach number and the flight path angle of the vehicle using control inputs of fuel-to-air ratio ϕ and elevator deflection δ_e. To achieve this goal, it is simpler to substitute γ for $\theta - \alpha$. This gives the following equations.

$$\dot{M} = c_0(\alpha, M) + c_1(\alpha, M)\phi cos\alpha + c_2(M)\delta_e + c_3(M)\delta_e^2 - c_4 sin(\gamma) \tag{4.8}$$

$$\dot{\gamma} = c_5(\alpha) + \frac{c_1(\alpha, M)}{M}\phi sin\alpha - c_6(M)\delta_e - \frac{c_4}{M}cos(\gamma) + c_7 M cos(\gamma) \tag{4.9}$$

$$\dot{Q} = c_8(\alpha, M) + c_9(\alpha, M)\phi + c_{10}(M)\delta_e \tag{4.10}$$

$$\dot{h} = M v_s sin(\gamma) \tag{4.11}$$

$$\dot{\alpha} = Q - \dot{\gamma} \tag{4.12}$$

In order to determine the control inputs needed to achieve a constant Mach number and flight path angle, the dynamics expressed by the equations for $\dot{M}$ and $\dot{\gamma}$ are set equal to zero as shown below.

$$0 = c_0(\alpha, M) + c_1(\alpha, M)\phi cos\alpha + c_2(M)\delta_e + c_3(M)\delta_e^2 - c_4 sin(\gamma) \tag{4.13}$$

$$0 = c_5(\alpha) + \frac{c_1(\alpha, M)}{M}\phi sin\alpha - c_6(M)\delta_e - \frac{c_4}{M}cos(\gamma) + c_7 M cos(\gamma) \tag{4.14}$$

$$\dot{\alpha} = Q \tag{4.15}$$

Using only the equations for $\dot{M}$ and $\dot{\gamma}$ we can determine the control inputs necessary to maintain Mach number and flight path angle. Both equations depend on both control inputs.

Eliminating one of the control inputs from the two equations would allow an easy solution for the remaining control input. Multiplying the equation for $\dot{M}$ by $sin\alpha$ gives the following expression.

$$0 = sin\alpha \left[c_0(\alpha, M) + c_1(\alpha, M)\phi cos\alpha + c_2(M)\delta_e + c_3(M)\delta_e^2 - c_4 sin(\gamma)\right] \tag{4.16}$$

Multiplying the equation for $\dot{\gamma}$ by $Mcos\alpha$ gives the following expression.

$$0 = Mcos\alpha \left[c_5(\alpha) + \frac{c_1(\alpha, M)}{M}\phi sin\alpha - c_6(M)\delta_e - \frac{c_4}{M}cos(\gamma) + c_7 Mcos(\gamma)\right] \tag{4.17}$$

Subtracting one equation from the other can cancel all terms including the control input ϕ, therefore reducing the number of unknown control inputs present to one. This subtraction is shown below.

$$\begin{aligned} &sin\alpha \left[c_0(\alpha, M) + c_1(\alpha, M)\phi cos\alpha + c_2(M)\delta_e + c_3(M)\delta_e^2 - c_4 sin(\gamma)\right] \\ &\quad - cos\alpha \left[c_5(\alpha)M + c_1(\alpha, M)\phi sin\alpha - c_6(M)\delta_e M - c_4 cos(\gamma) + c_7 M^2 cos(\gamma)\right] = 0 \end{aligned} \tag{4.18}$$

The common terms disappear and the expression becomes.

$$\begin{aligned} &sin\alpha \left[c_0(\alpha, M) + c_2(M)\delta_e + c_3(M)\delta_e^2 - c_4 sin(\gamma)\right] \\ &\qquad - cos\alpha \left[c_5(\alpha)M - c_6(M)\delta_e M - c_4 cos(\gamma) + c_7 M^2 cos(\gamma)\right] = 0 \end{aligned} \tag{4.19}$$

Multiplying the $sin\alpha$ and $cos\alpha$ terms through forms the following equation.

$$\begin{aligned} &c_0(\alpha, M)sin\alpha + c_2(M)\delta_e sin\alpha + c_3(M)\delta_e^2 sin\alpha - c_4 sin(\gamma)sin\alpha - c_5(\alpha)Mcos\alpha + c_6(M)\delta_e Mcos\alpha \\ &\qquad + c_4 cos(\gamma)cos\alpha - c_7 M^2 cos(\gamma)cos\alpha = 0 \end{aligned} \tag{4.20}$$

This equation can be simplified using the trig identity $cos(u + v) = cosucosv - sinusinv$. The simplified equation is given below.

$$\begin{aligned} &c_3(M)\delta_e^2 sin\alpha + c_2(M)\delta_e sin\alpha + c_6(M)\delta_e Mcos\alpha + c_0(\alpha, M)sin\alpha \\ &\qquad - c_5(\alpha)Mcos\alpha + c_4 cos(\gamma + \alpha) - c_7 M^2 cos(\gamma)cos\alpha = 0 \end{aligned} \tag{4.21}$$

The TM is defined over the domain $\alpha \in [-5, 10]$ degrees. As the model is only valid for relatively small angles of attack, it is assumed that $sin\alpha \approx \alpha$ and $cos\alpha \approx 1$. This assumption reduces the equation to the following form.

$$c_3(M)\delta_e^2\alpha + c_2(M)\delta_e\alpha + c_6(M)\delta_e M + c_0(\alpha, M)\alpha - c_5(\alpha)M + c_4 cos(\gamma + \alpha) - c_7 M^2 cos(\gamma) = 0 \tag{4.22}$$

The equation above is a quadratic equation in terms of the single control input δ_e. This quadratic equation has the following form.

$$A\delta_e^2 + B\delta_e + C = 0 \tag{4.23}$$

The variables A, B, and C in the equation above are representatives of the coefficients below.

$$A = c_3(M)\alpha \tag{4.24}$$

$$B = c_2(M)\alpha + c_6(M)M \tag{4.25}$$

$$C = c_0(\alpha, M)\alpha - c_5(\alpha)M + c_4 cos(\gamma + \alpha) - c_7 M^2 cos(\gamma) \tag{4.26}$$

The advantage of having a quadratic equation in terms of δ_e is the ability to solve such an equation easily using the quadratic formula. The solutions for the control input δ_e needed to maintain a constant Mach number and flight path angle are shown below.

$$\delta_e = \frac{-B \pm \sqrt{B^2 - 4AC}}{2A} \tag{4.27}$$

These solutions for the δ_e required to maintain a specified Mach number and flight path angle do not depend on the second control input ϕ. Both of the two solutions for δ_e are valid control inputs (within the vehicle's elevator deflection capability at trim conditions). The solutions for δ_e have singularities when $A = 0$. Either the angle of attack or $c_3(\alpha)$ would need to be zero for the singularity to occur. While an angle of attack of zero is within the flight envelope of the hypersonic vehicle, it is not included in any of the vehicle's trim conditions where $\gamma = 0$. Therefore if control inputs are applied to maintain a flight path angle of zero

at a trim condition then the angle of attack would theoretically not be equal to zero and would not create a singularity. However, because the trim conditions examined in this thesis are found using the 'fmincon' function and are therefore not exact, the α could potentially change and become equal to zero, thus creating a singularity. $c_3(\alpha)$ is dependent on the vehicle's drag independent of the control inputs. This drag will never be zero, and therefore $c_3(\alpha)$ will not create a singularity.

It is now possible to solve for the ϕ required to maintain the same Mach number and flight path angle using the original equation for $\dot{\gamma}$. This solution is shown below.

$$0 = c_5(\alpha) + \frac{c_1(\alpha, M)}{M}\phi sin\alpha - c_6(M)\delta_e - \frac{c_4}{M}cos(\gamma) + c_7 M cos(\gamma) \tag{4.28}$$

$$\phi = \frac{M\left[-c_5(\alpha) + c_6(M)\delta_e + \frac{c_4}{M}cos(\gamma) - c_7 M cos(\gamma)\right]}{c_1(\alpha, M)sin\alpha} \tag{4.29}$$

Substituting the two different solutions for δ_e into the equation for ϕ yields two solutions for ϕ. Only one of the solutions is a valid control input for the vehicle at trim conditions. Therefore one of the solution sets for the two control inputs is determined to be invalid and the following equations are the correct expressions for the control inputs required to maintain a commanded Mach number and flight path angle.

$$\delta_e = \frac{-\left(c_2(M)\alpha + c_6(M)M\right)}{2\left(c_3(M)\alpha\right)} + \frac{\sqrt{\left(c_2(M)\alpha + c_6(M)M\right)^2 - 4\left(c_3(M)\alpha\right)\left(c_0(\alpha, M)\alpha - c_5(\alpha)M + c_4 cos(\gamma + \alpha) - c_7 M^2 cos(\gamma)\right)}}{2\left(c_3(M)\alpha\right)} \tag{4.30}$$

$$\phi = \frac{M\left[-c_5(\alpha) + c_6(M)\delta_e + \frac{c_4}{M}cos(\gamma) - c_7 M cos(\gamma)\right]}{c_1(\alpha, M)sin\alpha} \tag{4.31}$$

The above solution for ϕ has a singularity when $\alpha = 0$ or when $c_1(\alpha, M) = 0$. As stated above, $\alpha = 0$ could create a singularity. $c_1(\alpha, M)$ is essentially a measure of the coefficient of thrust dependent on ϕ. This coefficient is never equal to zero, and therefore $c_1(\alpha)$ would not create a singularity.

Now the control inputs needed to achieve a constant Mach number and pitch angle have been determined as a function of α and the states to be controlled (γ, M). One must examine the effects of these control inputs on the system's internal dynamics. Substituting these control inputs into the equations of motion gives the following dynamics.

$$\dot{M} = 0 \tag{4.32}$$

$$\dot{\gamma} = 0 \tag{4.33}$$

$$\dot{Q} = c_8(\alpha, M) + c_9(\alpha, M)\phi + c_{10}(M)\delta_e \tag{4.34}$$

$$\dot{h} = 0 \tag{4.35}$$

$$\dot{\alpha} = Q \tag{4.36}$$

In these dynamics, $\dot{Q}$ is only a function of α, γ, and M. The dynamics of the pitch rate state are shown below.

$$\dot{Q} = \ddot{\alpha} = c_8(\alpha, M) + c_9(\alpha, M)\phi + c_{10}(M)\delta_e \tag{4.37}$$

This equation describing $\dot{Q}$ is essentially a second order differential equation. If γ and M are considered as constant choices then the equation for $\dot{Q}$ can be described by the following form.

$$\ddot{\alpha}(t) + f(\alpha(t)) = 0 \tag{4.38}$$

In this expression $f(\alpha(t))$ is the function of alpha described by the entire right hand side of the equation for $\dot{Q}$. This equation is in the form of a simple harmonic oscillator. This undamped system is not stable. Therefore the internal dynamics of this system are unstable, and the system can be classified as non-minimum phase.

To further this analysis, a simulation was run using the control inputs found to stabilize M and γ. The simulation was run at the trim condition given in Table 4.1.

Table 4.1: Initial Condition for Zero Dynamics Simulation.

State	Initial Value
M_0	10.75
α_0	0.3153 deg
γ_0	0 deg
Q_0	0 deg/s
h_0	98859 ft

The results of this simulation are shown in Figure 4.2. As expected, the control inputs determined to maintain Mach number and flight path angle initially achieve their goal as M and γ remain stable. However, the internal states α and Q are uncontrolled. These states prove to be unstable as they begin exponentially increasing and reach large values within approximately 1 second. The simulation breaks down as these states go to infinity. These unstable zero dynamics exhibit the behavior of a non-minimum phase system.

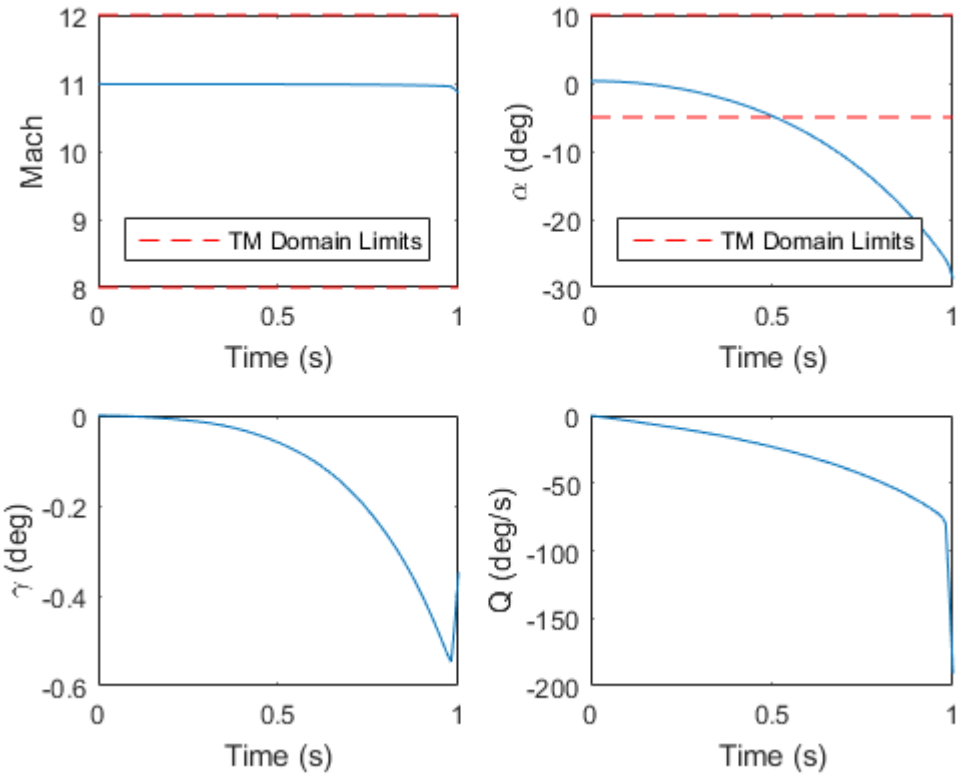

Figure 4.2: Time Simulation with Zero Dynamics Control Inputs Applied.

4.3 Control Design using the Indirect Manifold Construction Approach

The control objective is to drive the two outputs to desired reference points in finite time while ensuring that the internal states remain stable. This can be accomplished using the Indirect Manifold Construction approach developed by Narang-Siddarth and Valasek in 2014.[15] A diagram of the Indirect Manifold Construction approach is shown in Figure 4.3. The control design using this approach has three steps which are described in detail in the following subsections. In Step 1, the internal dynamics are assumed to be stable values while the output states are driven to commanded values. In Step 2, the first of the internal states is

driven to its assumed stable value while the other internal state is still assumed to be some stable value. In Step 3, the final internal state is driven to its assumed stable value.

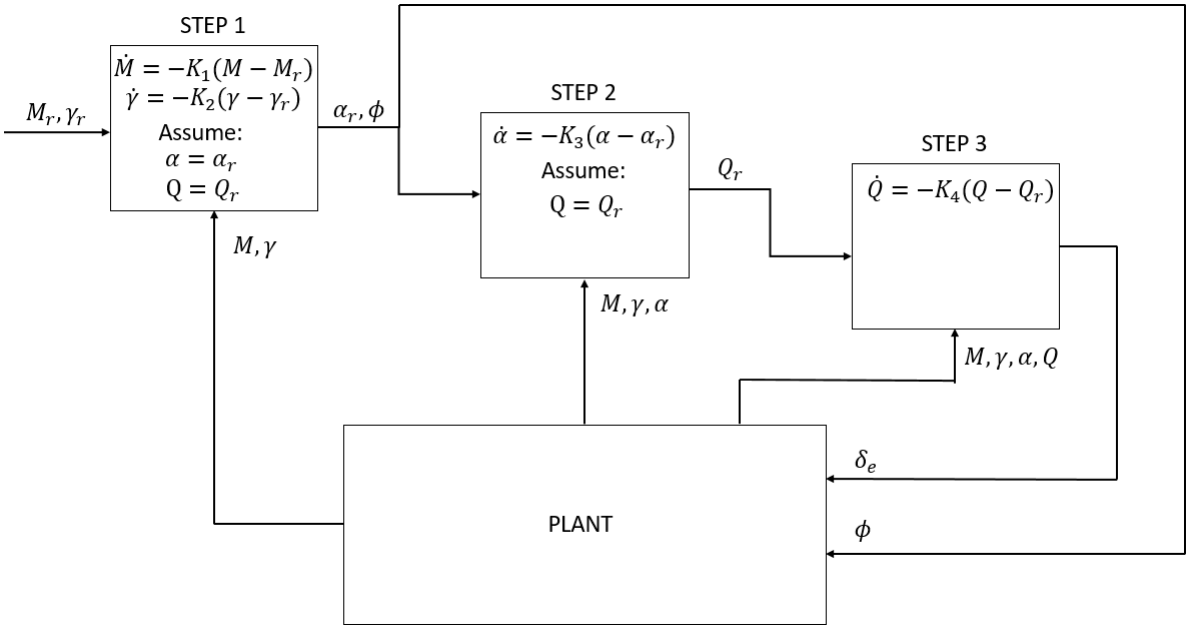

Figure 4.3: Indirect Manifold Construction Approach.

4.3.1 Step 1

To begin it is assumed that the vehicle is flying at a certain reference condition. This specified reference condition is a commanded M_r and γ_r. At this condition, some reference control input δ_{e_ζ} is required and the internal states are assumed to have settled down to the steady state values Q_r and α_r. Under this assumption the dynamics of the system become the

following equations.

$$\dot{M} = c_0(\alpha_r, M) + c_1(\alpha_r, M)\phi cos\alpha_r + c_2(M)\delta_{e_\zeta} + c_3(M)\delta_{e_\zeta}^2 - c_4 sin(\gamma) \tag{4.39}$$

$$\dot{\gamma} = c_5(\alpha_r) + \frac{c_1(\alpha_r, M)}{M}\phi sin\alpha_r - c_6(M)\delta_{e_\zeta} - \frac{c_4}{M}cos(\gamma) + c_7 M cos(\gamma) \tag{4.40}$$

$$0 = c_8(\alpha_r, M) + c_9(\alpha_r, M)\phi + c_{10}(M)\delta_{e_\zeta} \tag{4.41}$$

$$0 = Q_r - \dot{\gamma} \tag{4.42}$$

The goal is to drive M and γ to M_r and γ_r. This can be accomplished using the output feedback shown below.

$$\dot{M} = -K_1(M - M_r) \tag{4.43}$$

$$\dot{\gamma} = -K_2(\gamma - \gamma_r) \tag{4.44}$$

In this feedback loop, K_1 and K_2 are some constants which are design choices. With this feedback applied, the dynamics become the following equations.

$$-K_1(M - M_r) = c_0(\alpha_r, M) + c_1(\alpha_r, M)\phi cos\alpha_r + c_2(M)\delta_{e_\zeta} + c_3(M)\delta_{e_\zeta}^2 - c_4 sin(\gamma) \tag{4.45}$$

$$-K_2(\gamma - \gamma_r) = c_5(\alpha_r) + \frac{c_1(\alpha_r, M)}{M}\phi sin\alpha_r - c_6(M)\delta_{e_\zeta} - \frac{c_4}{M}cos(\gamma) + c_7 M cos(\gamma) \tag{4.46}$$

$$\tag{4.47}$$

From these equations, the required α_r and ϕ needed to make the dynamics valid can be solved for as shown below.

$$\phi = \frac{-K_1(M - M_r) - c_0(\alpha_r, M) - c_2(M)\delta_{e_\zeta} - c_3(M)\delta_{e_\zeta}^2 + c4 sin(\gamma)}{c_1(\alpha_r, M) cos\alpha_r} \tag{4.48}$$

$$sin\alpha_r = \frac{M\left[-K_2(\gamma - \gamma_r) - c_5(\alpha_r) + c_6(M)\delta_{e_\zeta} + \frac{c_4}{M}cos(\gamma) - c_7 M cos(\gamma)\right]}{c_1(\alpha_r, M)\phi} \tag{4.49}$$

These expressions for ϕ and α_r are in terms of $M, M_r, \gamma, \gamma_r, \alpha_r, \delta_{e_\zeta}$. The variable coefficients $c_0(\alpha_r, M)$, $c_1(\alpha_r, M)$, and $c_5(\alpha_r, M)$ vary with α_r and M. Examining the values of these

coefficients may allow for a more exact solution for α_r and ϕ.

$$c_0(\alpha_r, M) = \frac{\bar{q}S}{mM^2v_s}(t_0 cos\alpha_r - d_0) \tag{4.50}$$

$$c_1(\alpha_r, M) = \frac{\bar{q}S}{mM^2v_s}t_1 \tag{4.51}$$

$$c_5(\alpha_r, M) = \frac{\bar{q}S}{mM^2v_s}(t_0 sin\alpha_r - l_0) \tag{4.52}$$

One may consider using an order analysis to simplify these terms. The values of the coefficients are driven by the functions of thrust, drag, and lift shown above. These "coefficient driver functions" are essentially the coefficients themselves with a factor of $\frac{\bar{q}S}{mM^2v_s}$ removed. The coefficient driver functions are the problematic functions that would be helpful to simplify. Therefore one may examine how the coefficient driver functions vary with angle of attack. The results of this variation over the entire angle of attack envelope of the TM are shown in Figure 4.4.

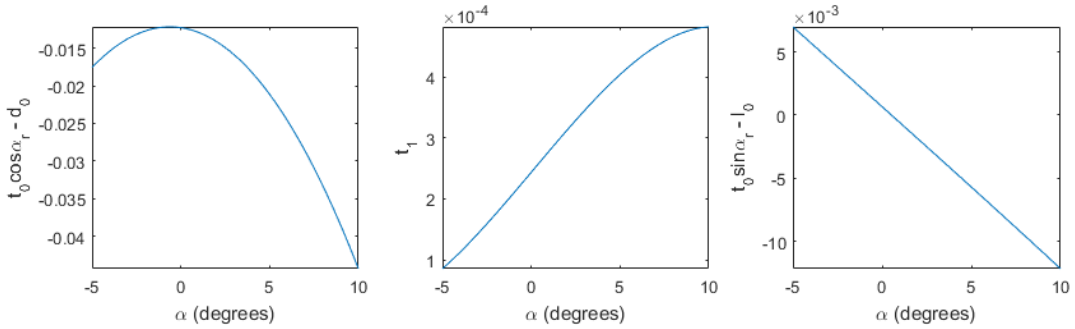

Figure 4.4: Variation of Coefficient Driver Functions over Flight Envelope.

The values of these coefficient driver functions can be approximated by simpler functions of α_r. The value of the driver function of $c_0(\alpha_r, M)$ is obviously not a linear function of α_r. Therefore that coefficient will be fit with a sinusoidal function. The value of the driver function of $c_1(\alpha_r, M)$ is not exactly a linear function of α_r, but it will be approximated by a linear function to greatly simplify the final solutions of interest (solutions for the control

inputs). The value of the driver function of $c_5(\alpha_r, M)$ is nearly a linear function of α_r and it will be approximated by a linear function. These approximations are shown as curve fits in Figure 4.5.

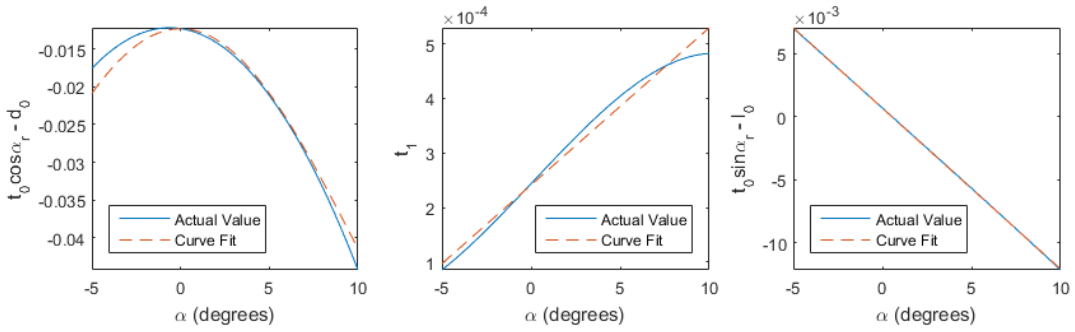

Figure 4.5: Variation of Coefficient Driver Functions over Flight Envelope.

The sinusoidal fit and first order polynomial curve fits of the coefficient driver functions are shown below, where s_i and p_i represent the values of the constants used in the curve fits.

$$t_0 cos\alpha_r - d_0 \approx s_1 cos\left(\frac{\alpha_r}{s_2}\right) + s_3 \tag{4.53}$$

$$t_1 \approx p_4\alpha_r + p_5 \tag{4.54}$$

$$t_0 sin\alpha_r - l_0 \approx p_6\alpha_r + p_7 \tag{4.55}$$

Substitution of these approximations into the equations for α_r and ϕ yield the equations shown below.

$$cos\alpha_r = \frac{-K_1(M - M_r) - \frac{\bar{q}S}{mv_s}(s_1 cos\left(\frac{\alpha_r}{s_2}\right) + s_3) - c_2(M)\delta_{e_\zeta} - c_3(M)\delta_{e_\zeta}^2 + c4sin(\gamma)}{\frac{\bar{q}S}{mv_s}(p_4\alpha_r + p_5)\,\phi} \tag{4.56}$$

$$\phi = \frac{M\left[-K_2(\gamma - \gamma_r) - \frac{\bar{q}S}{mMv_s}(p_6\alpha_r + p_7) + c_6(M)\delta_{e_\zeta} + \frac{c_4}{M}cos(\gamma) - c_7 M cos(\gamma)\right]}{\frac{\bar{q}S}{mv_s}(p_4\alpha_r + p_5)\,sin\alpha_r} \tag{4.57}$$

Both α_r and ϕ still depend on each other. However, because there are two equations and two unknowns one can solve for α_r and ϕ as shown below. To simplify analysis, the following representations are introduced.

$$z_1 = -K_1(M - M_r) - \frac{\bar{q}S}{mv_s}s_3 - c_2(M)\delta_{e_\zeta} - c_3(M)\delta_{e_\zeta}^2 + c4sin(\gamma) \tag{4.58}$$

$$z_2 = -MK_2\left(\gamma - \gamma_r\right) - \frac{\bar{q}S}{mv_s}p_7 + Mc_6(M)\delta_{e_\zeta} + c_4cos(\gamma) - M^2c_7cos(\gamma) \tag{4.59}$$

Substituting z_1 and z_2 into the expressions for α_r and ϕ gives the following equations.

$$\phi = \frac{z_1 - \left(\frac{\bar{q}S}{mv_s}\left(s_1 cos\left(\frac{\alpha_r}{s_2}\right)\right)\right)}{\left(\frac{\bar{q}S}{mv_s}\left(p_4\alpha_r + p_5\right)\right)cos\alpha_r} \tag{4.60}$$

$$sin\alpha_r = \frac{z_2 - \left(\frac{\bar{q}S}{mv_s}\left(p_6\alpha_r\right)\right)}{\left(\frac{\bar{q}S}{mv_s}\left(p_4\alpha_r + p_5\right)\right)\phi} \tag{4.61}$$

An assumption that α_r is small can be made and therefore $cos\alpha_r \approx cos\left(\frac{\alpha_r}{s_2}\right) \approx 1$ and $sin\alpha_r \approx \alpha_r$.

$$\phi = \frac{z_1 - \left(\frac{\bar{q}S}{mv_s}\left(s_1\right)\right)}{\left(\frac{\bar{q}S}{mv_s}\left(p_4\alpha_r + p_5\right)\right)} \tag{4.62}$$

$$\alpha_r = \frac{z_2 - \left(\frac{\bar{q}S}{mv_s}\left(p_6\alpha_r\right)\right)}{\left(\frac{\bar{q}S}{mv_s}\left(p_4\alpha_r + p_5\right)\right)\phi} \tag{4.63}$$

Substituting the equation for ϕ into the equation for $cos\alpha_r$ allows a solution for α_r to be

found as shown below.

$$\alpha_r = \frac{z_2 - \left(\frac{\bar{q}S}{mv_s}\left(p_6\alpha_r\right)\right)}{\left(\frac{\bar{q}S}{mv_s}\left(p_4\alpha_r + p_5\right)\right)\left[\frac{z_1 - \left(\frac{\bar{q}S}{mv_s}\left(s_1\right)\right)}{\left(\frac{\bar{q}S}{mv_s}\left(p_4\alpha_r + p_5\right)\right)}\right]} \tag{4.64}$$

$$\alpha_r = \frac{z_2 - \left(\frac{\bar{q}S}{mv_s}\left(p_6\alpha_r\right)\right)}{z_1 - \left(\frac{\bar{q}S}{mv_s}\left(s_1\right)\right)} \tag{4.65}$$

$$\alpha_r + \frac{\left(\frac{\bar{q}S}{mv_s}\left(p_6\alpha_r\right)\right)}{z_1 - \left(\frac{\bar{q}S}{mv_s}\left(s_1\right)\right)} = \frac{z_2}{z_1 - \left(\frac{\bar{q}S}{mv_s}\left(s_1\right)\right)} \tag{4.66}$$

$$\alpha_r\left(1 + \frac{\left(\frac{\bar{q}S}{mv_s}\left(p_6\right)\right)}{z_1 - \left(\frac{\bar{q}S}{mv_s}\left(s_1\right)\right)}\right) = \frac{z_2}{z_1 - \left(\frac{\bar{q}S}{mv_s}\left(s_1\right)\right)} \tag{4.67}$$

$$\alpha_r = \frac{\frac{z_2}{z_1 - \left(\frac{\bar{q}S}{mv_s}\left(s_1\right)\right)}}{\left(1 + \frac{\left(\frac{\bar{q}S}{mv_s}\left(p_6\right)\right)}{z_1 - \left(\frac{\bar{q}S}{mv_s}\left(s_1\right)\right)}\right)} \tag{4.68}$$

$$\alpha_r = \frac{z_2}{\left(1 + \frac{\left(\frac{\bar{q}S}{mv_s}\left(p_6\right)\right)}{z_1 - \left(\frac{\bar{q}S}{mv_s}\left(s_1\right)\right)}\right)\left(z_1 - \left(\frac{\bar{q}S}{mv_s}\left(s_1\right)\right)\right)} \tag{4.69}$$

$$\alpha_r = \frac{z_2}{z_1 - \frac{\bar{q}S}{mv_s}s_1 + \frac{\bar{q}S}{mv_s}p_6} \tag{4.70}$$

The equation for ϕ can be expressed with α_r now a known quantity.

$$\phi = \frac{z_1 - \left(\frac{\bar{q}S}{mv_s}\left(s_1\right)\right)}{\left(\frac{\bar{q}S}{mv_s}\left(p_4\alpha_r + p_5\right)\right)} \tag{4.71}$$

4.3.2 Step 2

The next step in the hierarchical control design is to assume that Q has settled down to some Q_r and that some control input δ_{e_ψ} is being applied. The dynamics of one of the internal states, $\dot{\alpha}$, can be forced as shown below.

$$\dot{\alpha} = -K_3(\alpha - \alpha_r) \tag{4.72}$$

$$Q_r - \dot{\gamma} = -K_3(\alpha - \alpha_r) \tag{4.73}$$

Substituting the $\dot{\gamma}$ equation of motion gives the complete equation needed to solve for Q_r.

$$Q_r - c_5(\alpha) - \frac{c_1(\alpha, M)}{M}\phi sin\alpha + c_6(M)\delta_{e_\psi} + \frac{c_4}{M}cos(\gamma) - c_7 M cos(\gamma) = -K_3(\alpha - \alpha_r) \tag{4.74}$$

A solution for Q_r is now obtained in terms of $M, \gamma, \alpha, \alpha_r, \phi, \delta_{e_\psi}$.

$$Q_r = c_5(\alpha) + \frac{c_1(\alpha, M)}{M}\phi sin\alpha - c_6(M)\delta_{e_\psi} - \frac{c_4}{M}cos(\gamma) + c_7 M cos(\gamma) - K_3(\alpha - \alpha_r) \tag{4.75}$$

4.3.3 Step 3

The final step in the control design is forcing the dynamics of the second internal state, $\dot{Q}$.

$$\dot{Q} = -K_4(Q - Q_r) \tag{4.76}$$

The following equation is taken from the original equations of motion.

$$\dot{Q} = c_8(\alpha, M) + c_9(\alpha, M)\phi + c_{10}(M)\delta_e = -K_4(Q - Q_r) \tag{4.77}$$

A solution for the δ_e required to force the dynamics in the proper manner can now be explicitly stated.

$$\delta_e = \frac{1}{c_{10}(M)}[-K_4(Q - Q_r) - c_8(\alpha, M) - c_9(\alpha, M)\phi] \tag{4.78}$$

Along with the equation for δ_e, the interim control inputs δ_{e_ζ} and δ_{e_ψ} can also be solved for. δ_{e_ζ} is applied when $\alpha = \alpha_r$ and $Q = Q_r$ and δ_{e_ψ} is applied when $Q = Q_r$. The resulting solutions are shown below.

$$\delta_{e_\zeta} = \frac{1}{c_{10}(M)}[-c_8(\alpha_r, M) - c_9(\alpha_r, M)\phi] \tag{4.79}$$

$$\delta_{e_\psi} = \frac{1}{c_{10}(M)}[-c_8(\alpha, M) - c_9(\alpha, M)\phi] \tag{4.80}$$

4.3.4 Final Control Inputs

The final solutions for the control inputs are given below.

$$\phi = \frac{z_1 - \left(\frac{\bar{q}S}{mv_s}(s_1)\right)}{\left(\frac{\bar{q}S}{mv_s}(p_4\alpha_r + p_5)\right)} \tag{4.81}$$

$$\delta_e = \frac{1}{c_{10}(M)}[-K_4(Q - Q_r) - c_8(\alpha, M) - c_9(\alpha, M)\phi] \tag{4.82}$$

4.4 Simulation Results

The controller designed in the previous section proves effective in simulation. Consider the initial condition given in Table 4.2.

Beginning with the TM at a near trim condition, the controller attempted to achieve a commanded Mach number and flight path angle. The controller gains selected are shown in Table 4.3. The results of the simulation are shown in Figure 4.6.

In the simulation, the closed loop system successfully tracks the commanded outputs while ensuring that the internal dynamics remain stable. In response to a commanded increase in Mach number, ϕ is increased to its maximum value. The effects of thrust on the vehicle's pitching moment are large in simulation as expected. The non-minimum phase behavior of

Table 4.2: Initial Condition for Simulation.

State	Initial Value	Control Input	Initial Value
M_0	8.89	δ_{e_0}	10.64 deg
α_0	2.0397 deg	ϕ_0	0.7483
γ_0	0 deg		
Q_0	0 deg/s		
h_0	104,007 ft		

Table 4.3: Controller Gains used in Simulation.

Gain	Value
K_1	1
K_2	7
K_3	1
K_4	4

the system is apparent as well. As the thrust increases, a nose up pitching moment is created. A change in elevator deflection is then made to force a nose down pitching moment. These changes cause a small departure from level flight. Over time, the closed loop system returns to level flight. Likewise, the decrease in thrust needed when the vehicle is commanded to decelerate causes an initial nose down pitching moment. However an elevator input then reverses this behavior and the vehicle ultimately pitches up. An example of this behavior is shown in Figure 4.8, which is a zoomed in view of the flight path angle as the thrust is decreased to decelerate from Mach 10.5 to Mach 9.5. In this simulation, the vehicle reaches two separate trim conditions. Note that the vehicle is able to decrease Mach number more

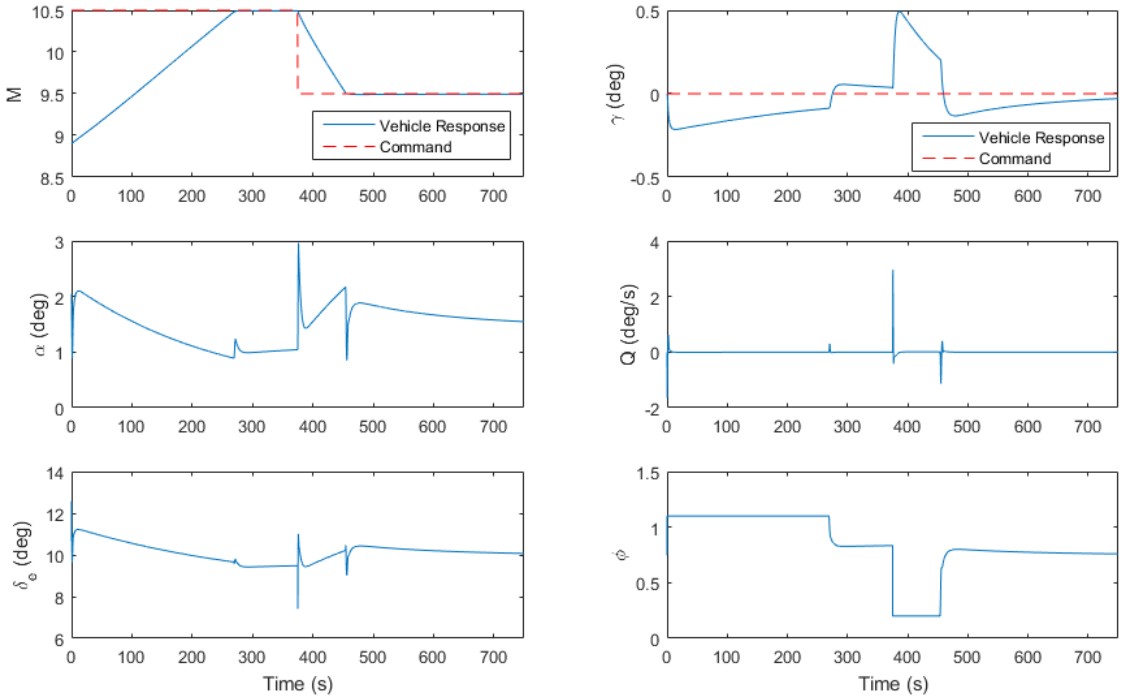

Figure 4.6: Time Simulation of the Closed Loop System.

quickly than increase Mach number. Over time, the controller returns the vehicle to level flight. The time scales needed to return to a level flight condition compare similarly to the time scales present in Fiorentini's closed loop simulation of the model with two control inputs.[14] The internal states (Q and α) remain stable throughout the entire simulation, as do the flexible states. The changes in the internal states appear to development very sharply. This development is not necessarily as sharp as it appears in Figure 4.6 as this behavior is caused by the internal states developing faster than the output states and the large time over which the simulation was run.

The non-minimum phase behavior of the closed loop system is also easily seen if the beginning of the simulation is observed closely. Figure 4.9 shows the first five seconds of the

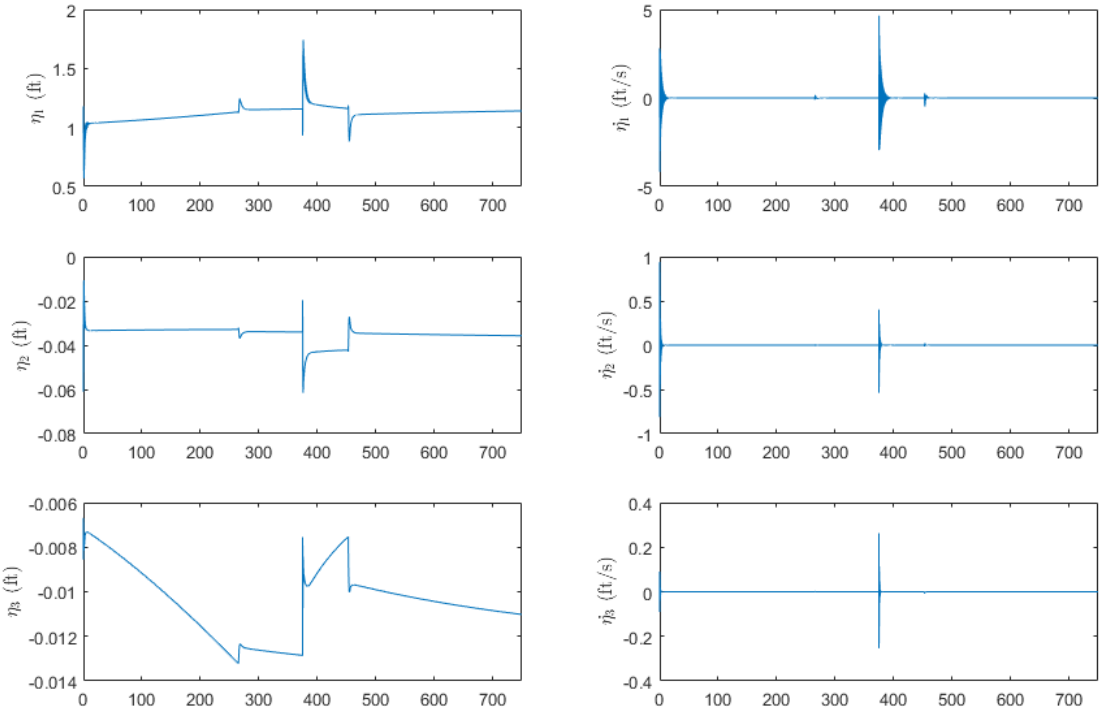

Figure 4.7: Time Simulation of the Closed Loop System.

closed loop simulation. The initial oscillation in pitch is typical of a non-minimum phase system.

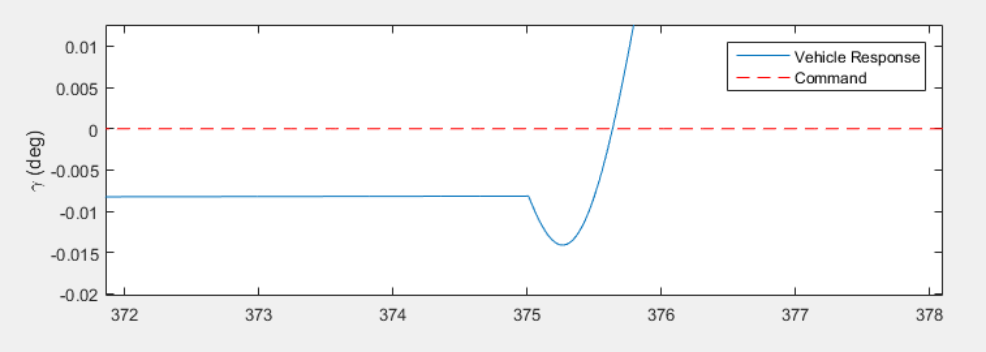

Figure 4.8: Non-Minimum Phase Behavior of Flight Path Angle.

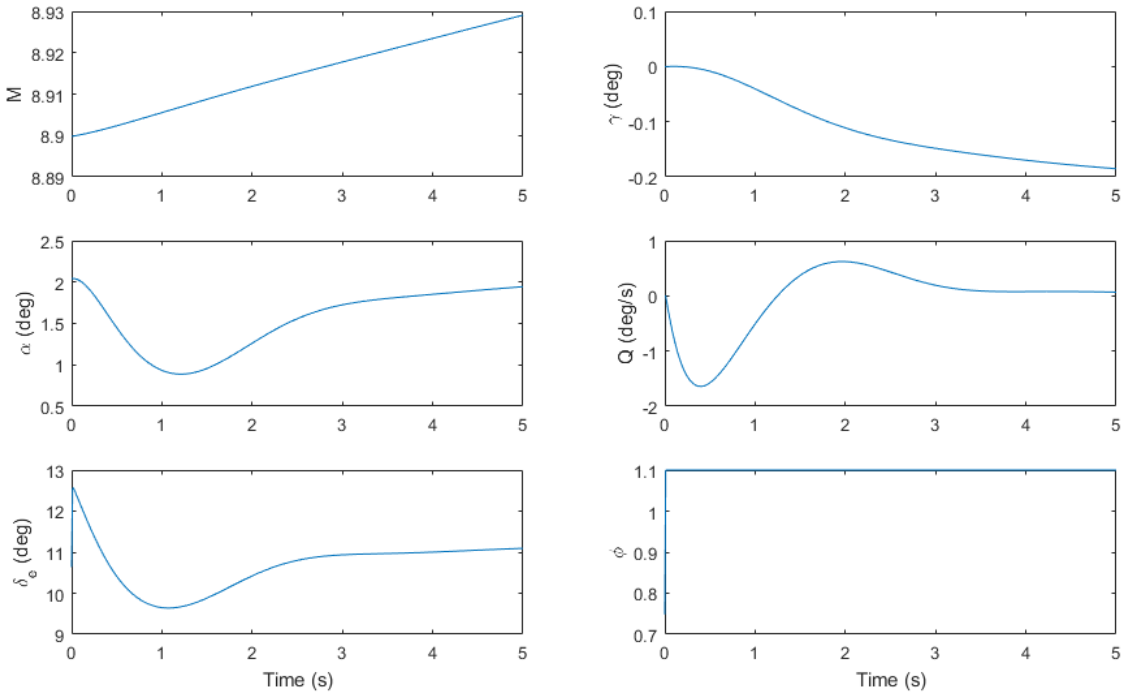

Figure 4.9: First Five Seconds of Time Simulation.

4.5 Lyapunov Stability Analysis

While the controller developed using the Indirect Manifold Construction approach is stable in simulation, more analysis is needed to choose controller gain values that guarantee stability. The following Theorem from Narang-Siddarth and Valasek[15] guarantees stability.

Theorem 1 (Stability Analysis) *Suppose the control* $\boldsymbol{u}(t, M, \gamma, \alpha, Q)$ *of a system is designed according to the Steps given previously. Then for all initial conditions* $(M, \gamma, \alpha, Q) \in D_M \; x \; D_\gamma \; x \; D_\alpha \; x \; D_Q$*, the control uniformly asymptotically stabilizes the nonlinear system and equivalently drives the internal dynamics to the* α_r *and* Q_r*.*

Theorem 1 will be proved using a Lyapunov based stability analysis. Slotine and Li provide the following "Lyapunov Theorem for Global Stability."[18]

Theorem 2 (Global Stability) *Assume that there exists a scalar function V of the state* $\boldsymbol{x}$*, with continuous first order derivatives such that*

- *V(x) is positive definite*
- $\dot{V}(x)$ *is negative definite*
- $V(x) \to \infty$ *as* $||x|| \to \infty$

then the equilibrium at the origin is globally asymptotically stable.

For the closed loop system, the following candidate Lyapunov Function is defined.

$$V = \frac{1}{2}(M - M_r)^2 + \frac{1}{2}(\gamma - \gamma_r)^2 + \frac{1}{2}(\alpha - \alpha_r)^2 + \frac{1}{2}(Q - Q_r)^2 \tag{4.83}$$

This function satisfies the first requirement of Theorem 1 as V(x) is positive definite. The derivative of this Lyapunov Function is shown below.

$$\dot{V} = (M - M_r)\dot{M} + (\gamma - \gamma_r)\dot{\gamma} + (\alpha - \alpha_r)(\dot{\alpha} - \dot{\alpha_r}) + (Q - Q_r)(\dot{Q} - \dot{Q}_r) \tag{4.84}$$

The derivative above is too complex to analytically prove negative definiteness. In order to prove negative definiteness, all of the terms of the derivative will be bounded individually

except for the control gains. By bounding these terms and organizing them into a matrix and applying the Lipschitz condition, the controller gains needed to guarantee stability can be found. The Lipschitz condition is given by Khalil as, $f(x,t)$ satisfies the inequality

$$||f(x,t) - f(t,y)|| \leq L||x-y|| \tag{4.85}$$

for all (t,x) and (t,y) in some neighborhood of (t_0,x_0).[19]

The first step in this analysis is to isolate the effects of each of the controller gains. In order to isolate the effects of the gain K_1 on the sign of $\dot{V}$, $\dot{M}$ is replaced in the following manner. First, a new term $\dot{M}_\rho$ is introduced.

$$\dot{M}|_{\alpha=\alpha_r, Q=Q_r} = \dot{M}_\rho \tag{4.86}$$

This new term allows the explicit separation of K_1 from $\dot{M}$ as shown below.

$$(M-M_r)\dot{M} = (M-M_r)\left[\dot{M}_\rho + \left(\dot{M} - \dot{M}_\rho\right)\right] \tag{4.87}$$

$$(M-M_r)\dot{M} = (M-M_r)\left[-K_1(M-M_r) + \left(\dot{M} - \dot{M}_\rho\right)\right] \tag{4.88}$$

Now the remaining terms that make up $\left(\dot{M} - \dot{M}_\rho\right)$ can be evaluated individually. These terms are shown below.

$$\begin{aligned}\dot{M} - \dot{M}_\rho = [c_0(\alpha,M) - c_0(\alpha_r,M)] + [c_1(\alpha,M)\phi cos\alpha - c_1(\alpha_r,M)\phi cos\alpha_r] \\ + \left[c_2(M)\delta_e - c_2(M)\delta_{e_\zeta}\right] + \left[c_3(M)\delta_e^2 - c_3(M)\delta_{e_\zeta}^2\right]\end{aligned} \tag{4.89}$$

By evaluating the terms above over the entire flight envelope of the hypersonic vehicle, upper bounds can be placed on the terms using linear functions. These linear bounding functions are shown below.

$$[c_0(\alpha,M) - c_0(\alpha_r,M)] < b_1(\alpha-\alpha_r) \tag{4.90}$$

$$[c_1(\alpha,M)\phi cos\alpha - c_1(\alpha_r,M)\phi cos\alpha_r] < b_2(\alpha-\alpha_r) \tag{4.91}$$

$$\left[c_2(M)\delta_e - c_2(M)\delta_{e_\zeta}\right] + \left[c_3(M)\delta_e^2 - c_3(M)\delta_{e_\zeta}^2\right] < b_3(\alpha-\alpha_r) \tag{4.92}$$

An example of the b_1 bounding function is shown in Figure 4.10. Note that the bounding function is very conservative, and thus robust to differences between assumed dynamics and true dynamics, imperfect state estimates, and uncertainties in aerodynamic and propulsive curve-fits.

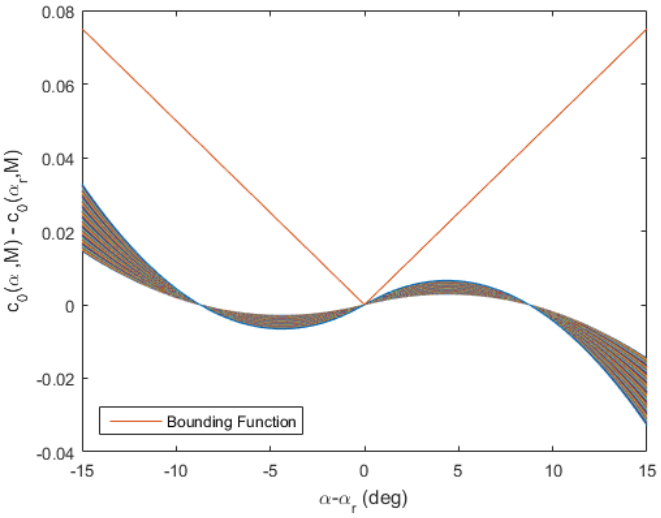

Figure 4.10: Bounding Function b_1.

Adding the bounding functions leads to the following expression.

$$\dot{M} - \dot{M}_\rho < (b_1 + b_2 + b_3)(\alpha - \alpha_r) \tag{4.93}$$

The expression for the $(M - M_r)\dot{M}$ term of $\dot{V}$ can now be organized into a form that will be convenient for matrix formation as shown below.

$$(M - M_r)\dot{M} = -K_1(M - M_r)^2 + (M - M_r)\left(\dot{M} - \dot{M}_\rho\right) \tag{4.94}$$

$$(M - M_r)\dot{M} < -K_1(M - M_r)^2 + (b_1 + b_2 + b_3)(\alpha - \alpha_r)(M - M_r) \tag{4.95}$$

The process taken above for K_1 needs to be repeated for the remaining controller gains. In order to isolate the effects of the gain K_2 on the sign of $\dot{V}$, $\dot{\gamma}$ is replaced in the following

manner. First, a new term $\dot{\gamma}_\rho$ is introduced.

$$\dot{\gamma}|_{\alpha=\alpha_r, Q=Q_r} = \dot{\gamma}_\rho \tag{4.96}$$

This new term allows the explicit separation of K_2 from $\dot{\gamma}$ as shown below.

$$(\gamma - \gamma_r)\dot{\gamma} = (\gamma - \gamma_r)\left[\dot{\gamma}_\rho + (\dot{\gamma} - \dot{\gamma}_\rho)\right] \tag{4.97}$$

$$(\gamma - \gamma_r)\dot{\gamma} = (\gamma - \gamma_r)\left[-K_2(\gamma - \gamma_r) + (\dot{\gamma} - \dot{\gamma}_\rho)\right] \tag{4.98}$$

Now the remaining terms that make up $(\dot{\gamma} - \dot{\gamma}_\rho)$ can be evaluated individually. These terms are shown below.

$$\dot{\gamma} - \dot{\gamma}_\rho = [c_5(\alpha) - c_5(\alpha_r)] + \left[\frac{c_1(\alpha, M)}{M}\phi sin\alpha - \frac{c_1(\alpha_r, M)}{M}\phi sin\alpha_r\right] + \left[-c_6(M)\delta_e + c_6(M)\delta_{e_\zeta}\right] \tag{4.99}$$

By evaluating the terms above over the entire flight envelope of the hypersonic vehicle, upper bounds can be placed on the terms using linear functions. These linear bounding functions are shown below.

$$[c_5(\alpha) - c_5(\alpha_r)] < b_4(\alpha - \alpha_r) \tag{4.100}$$

$$\left[\frac{c_1(\alpha, M)}{M}\phi sin\alpha - \frac{c_1(\alpha_r, M)}{M}\phi sin\alpha_r\right] < b_5(\alpha - \alpha_r) \tag{4.101}$$

$$\left[-c_6(M)\delta_e + c_6(M)\delta_{e_\zeta}\right] < b_6(\alpha - \alpha_r) \tag{4.102}$$

Adding the bounding functions leads to the following expression.

$$\dot{\gamma} - \dot{\gamma}_\rho < (b_4 + b_5 + b_6)(\alpha - \alpha_r) \tag{4.103}$$

The expression for the $(\gamma - \gamma_r)\dot{\gamma}$ term of $\dot{V}$ can now be organized into a form that will be convenient for matrix formation as shown below.

$$(\gamma - \gamma_r)\dot{\gamma} = -K_2(\gamma - \gamma_r)^2 + (\gamma - \gamma_r)\left(\dot{\gamma} - \dot{\gamma}_\rho\right) \tag{4.104}$$

$$(\gamma - \gamma_r)\dot{\gamma} < -K_2(\gamma - \gamma_r)^2 + (b_4 + b_5 + b_6)(\alpha - \alpha_r)(\gamma - \gamma_r) \tag{4.105}$$

In order to isolate the effects of the gain K_3 on the sign of $\dot{V}$, $\dot{\alpha} - \dot{\alpha}_r$ is replaced in the following manner. The first step in this process will be to replace the terms in $\dot{\alpha}$ with bounding functions. A new term $\dot{\alpha}_\rho$ is introduced.

$$\dot{\alpha}|_{Q=Q_r} = \dot{\alpha}_\rho \tag{4.106}$$

This new term allows the explicit separation of K_3 from $\dot{\alpha} - \dot{\alpha}_r$ as shown below.

$$(\alpha - \alpha_r)\dot{\alpha} = (\alpha - \alpha_r)\left[\dot{\alpha}_\rho + (\dot{\alpha} - \dot{\alpha}_\rho)\right] \tag{4.107}$$

$$(\alpha - \alpha_r)\dot{\alpha} = (\alpha - \alpha_r)\left[-K_3(\alpha - \alpha_r) + (\dot{\alpha} - \dot{\alpha}_\rho)\right] \tag{4.108}$$

Now the remaining terms that make up $(\dot{\alpha} - \dot{\alpha}_\rho)$ can be evaluated individually. These terms are shown below.

$$\dot{\alpha} - \dot{\alpha}_\rho = [Q - Q_r] + \left[c_6(M)\delta_e - c_6(M)\delta_{e_\psi}\right] \tag{4.109}$$

Evaluating the $\left[c_6(M)\delta_e - c_6(M)\delta_{e_\psi}\right]$ term over the entire flight envelope of the hypersonic vehicle, an upper bound can be placed on the term using a linear function. This linear bounding function is shown below.

$$\left[c_6(M)\delta_e - c_6(M)\delta_{e_\psi}\right] < b_7(\alpha - \alpha_r) \tag{4.110}$$

The equation for $(\alpha - \alpha_r)\dot{\alpha}$ can now be arranged into the following form.

$$(\alpha - \alpha_r)\dot{\alpha} = -K_3(\alpha - \alpha_r)^2 + (\alpha - \alpha_r)\left(\dot{\alpha} - \dot{\alpha}_\rho\right) \tag{4.111}$$

$$(\alpha - \alpha_r)\dot{\alpha} = -K_3(\alpha - \alpha_r)^2 + b_7(\alpha - \alpha_r)^2 + (\alpha - \alpha_r)\left[Q - Q_r\right] \tag{4.112}$$

Next the terms in $\dot{\alpha_r}$ must be replaced with bounding functions. Finding $\dot{\alpha_r}$ is a little more involved, as partial derivatives must be taken. The process of finding $\dot{\alpha_r}$ is shown below.

$$\alpha_r = \frac{z_2}{z_1 - \frac{\bar{q}S}{mv_s}s_1 + \frac{\bar{q}S}{mv_s}p_6} \tag{4.113}$$

$$\dot{\alpha}_r = \frac{\partial \alpha_r}{\partial M}\dot{M} + \frac{\partial \alpha_r}{\partial \gamma}\dot{\gamma} \tag{4.114}$$

$$\frac{\partial \alpha_r}{\partial M} = \frac{\left(-K_2(\gamma-\gamma_r) - \frac{\rho M v_s S}{m} p_7 \dot{M} + c_6(M)\delta_{e_\zeta}\frac{\rho v_s S l_1}{2m} - 2Mc_7 cos(\gamma)\dot{M}\right)\left(z_1 - \frac{\bar{q}S}{mv_s}s_1 + \frac{\bar{q}S}{mv_s}p_6\right)}{\left(z_1 - \frac{\bar{q}S}{mv_s}s_1 + \frac{\bar{q}S}{mv_s}p_6\right)^2} \\ \frac{-\left(-K_1 - \frac{\rho M v_s S}{m}s_3\dot{M} - \frac{\rho M v_s S d_1}{m}\delta_{e_\zeta}\dot{M} - \frac{\rho M v_s S d_2}{m}\delta_{e_\zeta}^2\dot{M} - \frac{\rho M v_s S}{m}s_1\dot{M} + \frac{\rho M v_s S}{m}p_6\dot{M}\right)z_2}{\left(z_1 - \frac{\bar{q}S}{mv_s}s_1 + \frac{\bar{q}S}{mv_s}p_6\right)^2} \tag{4.115}$$

$$\frac{\partial \alpha_r}{\partial \gamma} = \frac{\left(-MK_2 - c_4 sin(\gamma)\dot{\gamma} + M^2 c_7 sin(\gamma)\dot{\gamma}\right)\left(z_1 - \frac{\bar{q}S}{mv_s}s_1 + \frac{\bar{q}S}{mv_s}p_6\right) - \left(c_4 cos(\gamma)\dot{\gamma}\right)z_2}{\left(z_1 - \frac{\bar{q}S}{mv_s}s_1 + \frac{\bar{q}S}{mv_s}p_6\right)^2} \tag{4.116}$$

The terms that make up these partial derivatives must now be bounded as shown below.

$$\frac{-\rho M v_s S}{m}p_7 < b_8(M - M_r) \tag{4.117}$$

$$c_6(M)\delta_{e_\zeta}\frac{\rho v_s S l_1}{2m} < b_9(M - M_r) \tag{4.118}$$

$$-2Mc_7 cos(\gamma) < b_{10}(M - M_r) \tag{4.119}$$

$$z_1 = -K_1(M - M_r) - \frac{\bar{q}S}{mv_s}s_3 - c_2(M)\delta_{e_\zeta} - c_3(M)\delta_{e_\zeta}^2 + c4 sin(\gamma) \tag{4.120}$$

$$z_1 < -K_1(M - M_r) + b_{11}(M - M_r) + b_{12}(M - M_r) + b_{13}(M - M_r) \tag{4.121}$$

$$z_1 < -K_1(M - M_r) + (b_{11} + b_{12} + b_{13})(M - M_r) \tag{4.122}$$

$$z_2 = -MK_2\left(\gamma - \gamma_r\right) - \frac{\bar{q}S}{mv_s}p_7 + Mc_6(M)\delta_{e_\zeta} + c_4 cos(\gamma) - M^2 c_7 cos(\gamma) \tag{4.123}$$

$$z_2 < -8K_2\left(\gamma - \gamma_r\right) + b_{14}(M - M_r) + b_{15}(M - M_r) + b_{16}(\gamma - \gamma_r) + b_{17}(M - M_r) \tag{4.124}$$

$$z_2 < -8K_2\left(\gamma - \gamma_r\right) + (b_{14} + b_{15} + b_{17})(M - M_r) + b_{16}(\gamma - \gamma_r) \tag{4.125}$$

$$\left(-\frac{\bar{q}S}{mv_s}s_1 + \frac{\bar{q}S}{mv_s}p_6\right) < b_{18}(M - M_r) \tag{4.126}$$

$$\frac{-\rho M v_s S}{m}s_3 < b_{19}(M - M_r) \tag{4.127}$$

$$\frac{-\rho M v_s S d_1}{m}\delta_{e_\zeta} < b_{20}(M - M_r) \tag{4.128}$$

$$\frac{-\rho M v_s S d_2}{m}\delta_{e_\zeta}^2 < b_{21}(M - M_r) \tag{4.129}$$

$$\left(-\frac{\rho M v_s S}{m}s_1 + \frac{\rho M v_s S}{m}p_6\right) < b_{22}(M - M_r) \tag{4.130}$$

$$-c_4 sin(\gamma) < b_{23}(\gamma - \gamma_r) \tag{4.131}$$

$$M^2 c_7 sin(\gamma) < b_{24}(\gamma - \gamma_r) \tag{4.132}$$

$$-c_4 cos(\gamma) < b_{25}(\gamma - \gamma_r) \tag{4.133}$$

The partial derivatives can now be stated in the following form.

$$\begin{aligned}\frac{\partial \alpha_r}{\partial M} < & \frac{\left(-K_2(\gamma - \gamma_r) + b_8(M - M_r)\dot{M} + b_9(M - M_r) + b_{10}(M - M_r)\dot{M}\right)}{(-K_1(M - M_r) + (b_{11} + b_{12} + b_{13})(M - M_r) + b_{18}(M - M_r))} \\ & - \frac{\left(-K_1 + b_{19}(M - M_r)\dot{M} + b_{20}(M - M_r)\dot{M} + b_{21}(M - M_r)\dot{M} + b_{22}(M - M_r)\dot{M}\right)}{(-K_1(M - M_r) + (b_{11} + b_{12} + b_{13})(M - M_r) + b_{18}(M - M_r))^2} \\ & \frac{(-8K_2(\gamma - \gamma_r) + (b_{14} + b15 + b17)(M - M_r) + b_{16}(\gamma - \gamma_r))}{(-K_1(M - M_r) + (b_{11} + b_{12} + b_{13})(M - M_r) + b_{18}(M - M_r))^2}\end{aligned} \tag{4.134}$$

$$\begin{aligned}\frac{\partial \alpha_r}{\partial \gamma} < & \frac{(-8K_2 + (b_{23} + b_{24})(\gamma - \gamma_r)\dot{\gamma})\,(-K_1(M - M_r) + (b_{11} + b_{12} + b_{13} + b_{18})(M - M_r))}{(-K_1(M - M_r) + (b_{11} + b_{12} + b_{13})(M - M_r) + b_{18}(M - M_r))^2} \\ & \frac{+ (b_{25}(\gamma - \gamma_r)\dot{\gamma})\,(-8K_2(\gamma - \gamma_r) + (b_{14} + b15 + b17)(M - M_r) + b_{16}(\gamma - \gamma_r))}{(-K_1(M - M_r) + (b_{11} + b_{12} + b_{13})(M - M_r) + b_{18}(M - M_r))^2}\end{aligned} \tag{4.135}$$

These expressions can be reduced. First, the partial derivative of α_r with respect to M is

examined.

$$\frac{\partial \alpha_r}{\partial M} < \frac{\left(-K_2(\gamma-\gamma_r)+(b_8+b_{10})(M-M_r)\dot{M}+b_9(M-M_r)\right)}{((-K_1+b_{11}+b_{12}+b_{13}+b_{18})(M-M_r))} - \frac{\left(-K_1+(b_{19}+b_{20}+b_{21}+b_{22})(M-M_r)\dot{M}\right)}{((-K_1+b_{11}+b_{12}+b_{13}+b_{18})(M-M_r))^2} \frac{(-8K_2(\gamma-\gamma_r)+(b_{14}+b_{15}+b_{17})(M-M_r)+b_{16}(\gamma-\gamma_r))}{((-K_1+b_{11}+b_{12}+b_{13}+b_{18})(M-M_r))^2} \quad (4.136)$$

$$\frac{\partial \alpha_r}{\partial M} < \frac{-K_2(\gamma-\gamma_r)}{((-K_1+b_{11}+b_{12}+b_{13}+b_{18})(M-M_r))} + \frac{(b_8+b_{10})\dot{M}+b_9}{(-K_1+b_{11}+b_{12}+b_{13}+b_{18})} + \frac{K_1(b_{16}-8K_2)}{((-K_1+b_{11}+b_{12}+b_{13}+b_{18})(M-M_r))^2} - \frac{\left(-K_1(b_{14}+b_{15}+b_{17})+(8K_2+b_{16})(\gamma-\gamma_r)(b_{19}+b_{20}+b_{21}+b_{22})\dot{M}\right)}{(-K_1+b_{11}+b_{12}+b_{13}+b_{18})^2(M-M_r)} + \frac{\left((b_{19}+b_{20}+b_{21}+b_{22})(b_{14}+b_{15}+b_{17})\dot{M}\right)}{(-K_1+b_{11}+b_{12}+b_{13}+b_{18})^2} \quad (4.137)$$

The following bounded expression for $\dot{M}$ is needed.

$$\dot{M} < -K_1(M-M_r)+(b_1+b_2+b_3)(\alpha-\alpha_r) \quad (4.138)$$

$$\frac{\partial \alpha_r}{\partial M} < \frac{-K_2(\gamma-\gamma_r)}{((-K_1+b_{11}+b_{12}+b_{13}+b_{18})(M-M_r))}$$
$$+\frac{(b_8+b_{10})(-K_1(M-M_r)+(b_1+b_2+b_3)(\alpha-\alpha_r))+b_9}{(-K_1+b_{11}+b_{12}+b_{13}+b_{18})}$$
$$+\frac{K_1(b_{16}-8K_2)}{((-K_1+b_{11}+b_{12}+b_{13}+b_{18})(M-M_r))^2}$$
$$-\frac{-K_1(b_{14}+b_{15}+b_{17})}{(-K_1+b_{11}+b_{12}+b_{13}+b_{18})^2(M-M_r)}$$
$$+\frac{(8K_2+b_{16})(\gamma-\gamma_r)(b_{19}+b_{20}+b_{21}+b_{22})(-K_1(M-M_r)+(b_1+b_2+b_3)(\alpha-\alpha_r))}{(-K_1+b_{11}+b_{12}+b_{13}+b_{18})^2(M-M_r)}$$
$$+\frac{(b_{19}+b_{20}+b_{21}+b_{22})(b_{14}+b_{15}+b_{17})(-K_1(M-M_r)+(b_1+b_2+b_3)(\alpha-\alpha_r))}{(-K_1+b_{11}+b_{12}+b_{13}+b_{18})^2} \quad (4.139)$$

$$\frac{\partial \alpha_r}{\partial M} < \frac{-K_2(\gamma-\gamma_r)}{((-K_1+b_{11}+b_{12}+b_{13}+b_{18})(M-M_r))}$$
$$+\frac{(b_8+b_{10})(-K_1(M-M_r))}{(-K_1+b_{11}+b_{12}+b_{13}+b_{18})}$$
$$+\frac{(b_8+b_{10})(b_1+b_2+b_3)(\alpha-\alpha_r)}{(-K_1+b_{11}+b_{12}+b_{13}+b_{18})}$$
$$+\frac{b_9}{(-K_1+b_{11}+b_{12}+b_{13}+b_{18})}$$
$$+\frac{K_1(b_{16}-8K_2)}{((-K_1+b_{11}+b_{12}+b_{13}+b_{18})(M-M_r))^2}$$
$$-\frac{-K_1(b_{14}+b_{15}+b_{17})}{(-K_1+b_{11}+b_{12}+b_{13}+b_{18})^2(M-M_r)}$$
$$+\frac{(8K_2+b_{16})(\gamma-\gamma_r)(b_{19}+b_{20}+b_{21}+b_{22})(-K_1)}{(-K_1+b_{11}+b_{12}+b_{13}+b_{18})^2}$$
$$+\frac{(8K_2+b_{16})(\gamma-\gamma_r)(b_{19}+b_{20}+b_{21}+b_{22})(b_1+b_2+b_3)(\alpha-\alpha_r)}{(-K_1+b_{11}+b_{12}+b_{13}+b_{18})^2(M-M_r)}$$
$$+\frac{(b_{19}+b_{20}+b_{21}+b_{22})(b_{14}+b_{15}+b_{17})(-K_1(M-M_r))}{(-K_1+b_{11}+b_{12}+b_{13}+b_{18})^2}$$
$$+\frac{(b_{19}+b_{20}+b_{21}+b_{22})(b_{14}+b_{15}+b_{17})(b_1+b_2+b_3)(\alpha-\alpha_r)}{(-K_1+b_{11}+b_{12}+b_{13}+b_{18})^2} \quad (4.140)$$

Now multiplying this value by $\dot{M}$ gives the following term.

$$\begin{aligned}
\frac{\partial \alpha_r}{\partial M}\dot{M} < & \frac{K_1K_2(\gamma-\gamma_r)}{(-K_1+b_{11}+b_{12}+b_{13}+b_{18})} + \frac{-K_2(\gamma-\gamma_r)(b_1+b_2+b_3)(\alpha-\alpha_r)}{((-K_1+b_{11}+b_{12}+b_{13}+b_{18})(M-M_r))} \\
& + \frac{(b_8+b_{10})(K_1^2(M-M_r)^2)}{(-K_1+b_{11}+b_{12}+b_{13}+b_{18})} + \frac{(b_8+b_{10})(-K_1(M-M_r))(b_1+b_2+b_3)(\alpha-\alpha_r)}{(-K_1+b_{11}+b_{12}+b_{13}+b_{18})} \\
& + \frac{(b_8+b_{10})(b_1+b_2+b_3)(\alpha-\alpha_r)(-K_1(M-M_r))}{(-K_1+b_{11}+b_{12}+b_{13}+b_{18})} + \frac{(b_8+b_{10})(b_1+b_2+b_3)^2(\alpha-\alpha_r)^2}{(-K_1+b_{11}+b_{12}+b_{13}+b_{18})} \\
& + \frac{b_9(-K_1(M-M_r))}{(-K_1+b_{11}+b_{12}+b_{13}+b_{18})} + \frac{b_9(b_1+b_2+b_3)(\alpha-\alpha_r)}{(-K_1+b_{11}+b_{12}+b_{13}+b_{18})} \\
& + \frac{-K_1^2(b_{16}-8K_2)}{(-K_1+b_{11}+b_{12}+b_{13}+b_{18})^2(M-M_r)} + \frac{K_1(b_{16}-8K_2)(b_1+b_2+b_3)(\alpha-\alpha_r)}{(-K_1+b_{11}+b_{12}+b_{13}+b_{18})^2(M-M_r)^2} \\
& - \frac{K_1^2(b_{14}+b_{15}+b_{17})}{(-K_1+b_{11}+b_{12}+b_{13}+b_{18})^2} - \frac{-K_1(b_{14}+b_{15}+b_{17})(b_1+b_2+b_3)(\alpha-\alpha_r)}{(-K_1+b_{11}+b_{12}+b_{13}+b_{18})^2(M-M_r)} \\
& + \frac{(8K_2+b_{16})(\gamma-\gamma_r)(b_{19}+b_{20}+b_{21}+b_{22})(K_1^2)(M-M_r)}{(-K_1+b_{11}+b_{12}+b_{13}+b_{18})^2} \\
& + \frac{(8K_2+b_{16})(\gamma-\gamma_r)(b_{19}+b_{20}+b_{21}+b_{22})(-K_1)(b_1+b_2+b_3)(\alpha-\alpha_r)}{(-K_1+b_{11}+b_{12}+b_{13}+b_{18})^2} \\
& + \frac{(8K_2+b_{16})(\gamma-\gamma_r)(b_{19}+b_{20}+b_{21}+b_{22})(b_1+b_2+b_3)(\alpha-\alpha_r)}{(-K_1+b_{11}+b_{12}+b_{13}+b_{18})^2(M-M_r)} \\
& + \frac{(b_{19}+b_{20}+b_{21}+b_{22})(b_{14}+b_{15}+b_{17})(K_1(M-M_r))^2}{(-K_1+b_{11}+b_{12}+b_{13}+b_{18})^2} \\
& + \frac{(b_{19}+b_{20}+b_{21}+b_{22})(b_{14}+b_{15}+b_{17})(-K_1(M-M_r))(b_1+b_2+b_3)(\alpha-\alpha_r)}{(-K_1+b_{11}+b_{12}+b_{13}+b_{18})^2} \\
& + \frac{(b_{19}+b_{20}+b_{21}+b_{22})(b_{14}+b_{15}+b_{17})(b_1+b_2+b_3)(\alpha-\alpha_r)(-K_1(M-M_r))}{(-K_1+b_{11}+b_{12}+b_{13}+b_{18})^2} \\
& + \frac{(b_{19}+b_{20}+b_{21}+b_{22})(b_{14}+b_{15}+b_{17})(b_1+b_2+b_3)^2(\alpha-\alpha_r)^2}{(-K_1+b_{11}+b_{12}+b_{13}+b_{18})^2} \qquad (4.141)
\end{aligned}$$

In order to transition this term into a group of linear functions that will make up terms in the bound matrix, some of the difference terms have been replaced by their maximum values

as shown below.

$$\frac{\partial \alpha_r}{\partial M}\dot{M} < \frac{K_1K_2(\gamma-\gamma_r)}{(-K_1+b_{11}+b_{12}+b_{13}+b_{18})} + \frac{-K_2(\gamma-\gamma_r)(b_1+b_2+b_3)15}{((-K_1+b_{11}+b_{12}+b_{13}+b_{18})(4))}$$
$$+ \frac{(b_8+b_{10})(K_1^2 4(M-M_r))}{(-K_1+b_{11}+b_{12}+b_{13}+b_{18})} + \frac{(b_8+b_{10})(-K_1(M-M_r))(b_1+b_2+b_3)(15)}{(-K_1+b_{11}+b_{12}+b_{13}+b_{18})}$$
$$+ \frac{(b_8+b_{10})(b_1+b_2+b_3)(15)(-K_1(M-M_r))}{(-K_1+b_{11}+b_{12}+b_{13}+b_{18})} + \frac{(b_8+b_{10})(b_1+b_2+b_3)^2(15)(\alpha-\alpha_r)}{(-K_1+b_{11}+b_{12}+b_{13}+b_{18})}$$
$$+ \frac{b_9(-K_1(M-M_r))}{(-K_1+b_{11}+b_{12}+b_{13}+b_{18})} + \frac{b_9(b_1+b_2+b_3)(\alpha-\alpha_r)}{(-K_1+b_{11}+b_{12}+b_{13}+b_{18})}$$
$$+ \frac{-K_1^2(b_{16}-8K_2)(M-M_r)}{(-K_1+b_{11}+b_{12}+b_{13}+b_{18})^2(16)} + \frac{K_1(b_{16}-8K_2)(b_1+b_2+b_3)(\alpha-\alpha_r)}{(-K_1+b_{11}+b_{12}+b_{13}+b_{18})^2(16)}$$
$$- \frac{K_1^2(b_{14}+b_{15}+b_{17})(M-M_r)}{(-K_1+b_{11}+b_{12}+b_{13}+b_{18})^2(4)} - \frac{-K_1(b_{14}+b_{15}+b_{17})(b_1+b_2+b_3)(\alpha-\alpha_r)}{(-K_1+b_{11}+b_{12}+b_{13}+b_{18})^2(4)}$$
$$+ \frac{(8K_2+b_{16})(\gamma-\gamma_r)(b_{19}+b_{20}+b_{21}+b_{22})(K_1^2)(4)}{(-K_1+b_{11}+b_{12}+b_{13}+b_{18})^2}$$
$$+ \frac{(8K_2+b_{16})(\gamma-\gamma_r)(b_{19}+b_{20}+b_{21}+b_{22})(-K_1)(b_1+b_2+b_3)(15)}{(-K_1+b_{11}+b_{12}+b_{13}+b_{18})^2}$$
$$+ \frac{(8K_2+b_{16})(\gamma-\gamma_r)(b_{19}+b_{20}+b_{21}+b_{22})(b_1+b_2+b_3)(15)}{(-K_1+b_{11}+b_{12}+b_{13}+b_{18})^2(4)}$$
$$+ \frac{(b_{19}+b_{20}+b_{21}+b_{22})(b_{14}+b_{15}+b_{17})(K_1^2 4(M-M_r))}{(-K_1+b_{11}+b_{12}+b_{13}+b_{18})^2}$$
$$+ \frac{(b_{19}+b_{20}+b_{21}+b_{22})(b_{14}+b_{15}+b_{17})(-K_1(M-M_r))(b_1+b_2+b_3)(15)}{(-K_1+b_{11}+b_{12}+b_{13}+b_{18})^2}$$
$$+ \frac{(b_{19}+b_{20}+b_{21}+b_{22})(b_{14}+b_{15}+b_{17})(b_1+b_2+b_3)(15)(-K_1(M-M_r))}{(-K_1+b_{11}+b_{12}+b_{13}+b_{18})^2}$$
$$+ \frac{(b_{19}+b_{20}+b_{21}+b_{22})(b_{14}+b_{15}+b_{17})(b_1+b_2+b_3)^2 15(\alpha-\alpha_r)}{(-K_1+b_{11}+b_{12}+b_{13}+b_{18})^2} \quad (4.142)$$

Now the partial derivative of α_r with respect to γ will be examined.

$$\frac{\partial \alpha_r}{\partial \gamma} < \frac{(-8K_2 + (b_{23} + b_{24})(\gamma - \gamma_r)\dot{\gamma})\left((-K_1 + b_{11} + b_{12} + b_{13} + b_{18})(M - M_r)\right)}{\left((-K_1 + b_{11} + b_{12} + b_{13} + b_{18})(M - M_r)\right)^2} + \frac{(b_{25}(\gamma - \gamma_r)\dot{\gamma})\left((-8K_2 + b_{16})(\gamma - \gamma_r) + (b_{14} + b_{15} + b_{17})(M - M_r)\right)}{\left((-K_1 + b_{11} + b_{12} + b_{13} + b_{18})(M - M_r)\right)^2} \quad (4.143)$$

$$\frac{\partial \alpha_r}{\partial \gamma} < \frac{-8K_2(-K_1 + b_{11} + b_{12} + b_{13} + b_{18})(M - M_r)}{\left((-K_1 + b_{11} + b_{12} + b_{13} + b_{18})(M - M_r)\right)^2} + \frac{(b_{23} + b_{24})(\gamma - \gamma_r)\dot{\gamma}(-K_1 + b_{11} + b_{12} + b_{13} + b_{18})(M - M_r)}{\left((-K_1 + b_{11} + b_{12} + b_{13} + b_{18})(M - M_r)\right)^2} + \frac{(b_{25}\dot{\gamma})(-8K_2 + b_{16})(\gamma - \gamma_r)^2}{\left((-K_1 + b_{11} + b_{12} + b_{13} + b_{18})(M - M_r)\right)^2} + \frac{(b_{25}(\gamma - \gamma_r)\dot{\gamma})(b_{14} + b_{15} + b_{17})(M - M_r)}{\left((-K_1 + b_{11} + b_{12} + b_{13} + b_{18})(M - M_r)\right)^2} \quad (4.144)$$

The bounded expression for $\dot{\gamma}$ is needed.

$$\dot{\gamma} = -K_2(\gamma - \gamma_r) + (b_4 + b_5 + b_6)(\alpha - \alpha_r) \quad (4.145)$$

$$\frac{\partial \alpha_r}{\partial \gamma}\dot{\gamma} < \frac{-8K_2(-K_1+b_{11}+b_{12}+b_{13}+b_{18})}{(-K_1+b_{11}+b_{12}+b_{13}+b_{18})^2(M-M_r)}$$
$$+\frac{-K_2(b_{23}+b_{24})(\gamma-\gamma_r)^2(-K_1+b_{11}+b_{12}+b_{13}+b_{18})}{(-K_1+b_{11}+b_{12}+b_{13}+b_{18})^2(M-M_r)}$$
$$+\frac{(b_{23}+b_{24})(\gamma-\gamma_r)(b_4+b_5+b_6)(\alpha-\alpha_r)(-K_1+b_{11}+b_{12}+b_{13}+b_{18})}{(-K_1+b_{11}+b_{12}+b_{13}+b_{18})^2(M-M_r)}$$
$$+\frac{(-K_2b_{25})(-8K_2+b_{16})\left(\gamma-\gamma_r\right)^3}{(-K_1+b_{11}+b_{12}+b_{13}+b_{18})^2(M-M_r)^2}$$
$$+\frac{(b_{25}(b_4+b_5+b_6)(\alpha-\alpha_r))(-8K_2+b_{16})\left(\gamma-\gamma_r\right)^2}{(-K_1+b_{11}+b_{12}+b_{13}+b_{18})^2(M-M_r)^2}$$
$$+\frac{-K_2(b_{25}(\gamma-\gamma_r)^2)(b_{14}+b_{15}+b_{17})}{(-K_1+b_{11}+b_{12}+b_{13}+b_{18})^2(M-M_r)}$$
$$+\frac{(b_{25}(\gamma-\gamma_r)(b_4+b_5+b_6)(\alpha-\alpha_r))(b_{14}+b_{15}+b_{17})}{(-K_1+b_{11}+b_{12}+b_{13}+b_{18})^2(M-M_r)} \quad (4.146)$$

In order to transition this term into a group of linear functions that will make up terms in the bound matrix, some of the difference terms have been replaced by their maximum values

as shown below.

$$\begin{aligned}\frac{\partial \alpha_r}{\partial \gamma}\dot{\gamma} < & \frac{-8K_2(-K_1+b_{11}+b_{12}+b_{13}+b_{18})(M-M_r)}{(-K_1+b_{11}+b_{12}+b_{13}+b_{18})^2 16} \\ & + \frac{-K_2(b_{23}+b_{24})15(\gamma-\gamma_r)(-K_1+b_{11}+b_{12}+b_{13}+b_{18})}{(-K_1+b_{11}+b_{12}+b_{13}+b_{18})^2 4} \\ & + \frac{(b_{23}+b_{24})(\gamma-\gamma_r)(b_4+b_5+b_6)(15)(-K_1+b_{11}+b_{12}+b_{13}+b_{18})}{(-K_1+b_{11}+b_{12}+b_{13}+b_{18})^2(4)} \\ & + \frac{(-K_2 b_{25})(-8K_2+b_{16})225\,(\gamma-\gamma_r)}{(-K_1+b_{11}+b_{12}+b_{13}+b_{18})^2(16)} \\ & + \frac{(b_{25}(b_4+b_5+b_6)(15))(-8K_2+b_{16})15\,(\gamma-\gamma_r)}{(-K_1+b_{11}+b_{12}+b_{13}+b_{18})^2(16)} \\ & + \frac{-K_2(b_{25}(15)(\gamma-\gamma_r))(b_{14}+b_{15}+b_{17})}{(-K_1+b_{11}+b_{12}+b_{13}+b_{18})^2(4)} \\ & + \frac{(b_{25}(\gamma-\gamma_r)(b_4+b_5+b_6)(15))(b_{14}+b_{15}+b_{17})}{(-K_1+b_{11}+b_{12}+b_{13}+b_{18})^2(4)} \end{aligned} \tag{4.147}$$

After examining these partial derivatives of α_r, the process of bounding the following equation begins.

$$(\alpha-\alpha_r)\dot{\alpha}_r < (\alpha-\alpha_r)\left[\frac{\partial \alpha_r}{\partial M}\dot{M} + \frac{\partial \alpha_r}{\partial \gamma}\dot{\gamma}\right] \tag{4.148}$$

The $\dot{M}$ and $\dot{\gamma}$ can be replaced using the $\dot{M}_\rho$ and $\dot{\gamma}_\rho$ defined earlier.

$$(\alpha-\alpha_r)\dot{\alpha}_r < (\alpha-\alpha_r)\left[\frac{\partial \alpha_r}{\partial M}\left[\dot{M}_\rho + \left(\dot{M}-\dot{M}_\rho\right)\right] + \frac{\partial \alpha_r}{\partial \gamma}\left[\dot{\gamma}_\rho + (\dot{\gamma}-\dot{\gamma}_\rho)\right]\right] \tag{4.149}$$

$$(\alpha-\alpha_r)\dot{\alpha}_r < (\alpha-\alpha_r)\left[\frac{\partial \alpha_r}{\partial M}\left[-K_1(M-M_r) + \left(\dot{M}-\dot{M}_\rho\right)\right] + \frac{\partial \alpha_r}{\partial \gamma}\left[-K_2(\gamma-\gamma_r) + (\dot{\gamma}-\dot{\gamma}_\rho)\right]\right] \tag{4.150}$$

The $(\alpha - \alpha_r)(\dot{\alpha} - \dot{\alpha}_r)$ of the $\dot{V}$ equation is now given below.

$$(\alpha - \alpha_r)(\dot{\alpha} - \dot{\alpha}_r) < -K_3(\alpha - \alpha_r)^2 + (\alpha - \alpha_r)\left(\dot{\alpha} - \dot{\alpha}_\rho\right) - (\alpha - \alpha_r)\left[\frac{\partial \alpha_r}{\partial M}\dot{M} + \frac{\partial \alpha_r}{\partial \gamma}\dot{\gamma}\right] \quad (4.151)$$

In order to isolate the effects of the gain K_4, the final term of the $\dot{V}$ equation to be bounded is $(Q - Q_r)(\dot{Q} - \dot{Q}_r)$. The controller has been designed such that the dynamics of Q are as follows.

$$\dot{Q} = -K_4(Q - Q_r) \quad (4.152)$$

A bounded solution is needed for $\dot{Q}_r$.

$$\dot{Q}_r = \frac{\partial Q_r}{\partial M}\dot{M} + \frac{\partial Q_r}{\partial \gamma}\dot{\gamma} + \frac{\partial Q_r}{\partial \alpha}\dot{\alpha} \quad (4.153)$$

The terms in the expression above including partial derivatives are evaluated below.

$$\frac{\partial Q_r}{\partial M} = \left(-M^{-2}\right)\left(c_1(\alpha, M)\phi sin\alpha\right) + \frac{\rho v_s S t_1}{m}\phi sin\alpha\dot{M} - \frac{\rho v_s S l_1}{2m}\delta_{e_\psi}\dot{M} + M^{-2}c_4 cos(\gamma) + c_7 cos(\gamma) \quad (4.154)$$

$$\frac{\partial Q_r}{\partial \gamma} = \frac{c_4}{M}sin(\gamma)\dot{\gamma} - c_7 M sin(\gamma)\dot{\gamma} \quad (4.155)$$

$$\frac{\partial Q_r}{\partial \alpha} = -K_3 \quad (4.156)$$

The terms in the expressions above can be bounded as follows.

$$-M^{-2}(c_1(\alpha, M)\phi sin\alpha) < b_{26}(\alpha - \alpha_r) \quad (4.157)$$

$$\frac{\rho v_s S t_1}{m}\phi sin\alpha < b_{27}(\alpha - \alpha_r) \quad (4.158)$$

$$\frac{\rho v_s S l_1}{2m}\delta_{e_\psi} < b_{28}(M - M_r) \quad (4.159)$$

$$M^{-2}c_4 cos(\gamma) + c_7 cos(\gamma) < b_{29}(M - M_r) \quad (4.160)$$

$$\frac{c_4}{M}sin(\gamma) - c_7 M sin(\gamma) < b_{30}(\gamma - \gamma_r) \quad (4.161)$$

Placing these linear bounding terms into the partial derivatives gives the following equations.

$$\frac{\partial Q_r}{\partial M} < b_{26}(\alpha - \alpha_r) + b_{27}(\alpha - \alpha_r)\dot{M} + b_{28}(M - M_r)\dot{M} + b_{29}(M - M_r) \tag{4.162}$$

$$\frac{\partial Q_r}{\partial \gamma} < b_{30}(\gamma - \gamma_r)\dot{\gamma} \tag{4.163}$$

$$\frac{\partial Q_r}{\partial \alpha} < -K_3 \tag{4.164}$$

Replacing $\dot{M}$ and $\dot{\gamma}$ with their bounded approximations gives the following expressions.

$$\begin{aligned}\frac{\partial Q_r}{\partial M} < {} & b_{26}(\alpha - \alpha_r) - K_1(M - M_r)b_{27}(\alpha - \alpha_r) + (b_{27})(b_1 + b_2 + b_3)(\alpha - \alpha_r)^2 \\ & - K_1 b_{28}(M - M_r)^2 + b_{28}(b_1 + b_2 + b_3)(\alpha - \alpha_r)(M - M_r) + b_{29}(M - M_r)\end{aligned} \tag{4.165}$$

$$\frac{\partial Q_r}{\partial \gamma} < -K_2 b_{30}(\gamma - \gamma_r)^2 + b_{30}(\gamma - \gamma_r)(b_4 + b_5 + b_6)(\alpha - \alpha_r) \tag{4.166}$$

$$\frac{\partial Q_r}{\partial \alpha} < -K_3 \tag{4.167}$$

These partial derivatives must now be multiplied by $\dot{M}$, $\dot{\gamma}$, and $\dot{\alpha}$. The result of this multi-

plication is shown below.

$$\begin{aligned}\frac{\partial Q_r}{\partial M}\dot{M} < {} & (b_1+b_2+b_3)b_{26}(\alpha-\alpha_r)^2 - K_1 b_{26}(\alpha-\alpha_r)(M-M_r) \\ & + K_1^2(M-M_r)^2 b_{27}(\alpha-\alpha_r) - K_1(M-M_r)b_{27}(b_1+b_2+b_3)(\alpha-\alpha_r)^2 \\ & - K_1(M-M_r)(b_{27})(b_1+b_2+b_3)(\alpha-\alpha_r)^2 + (b_{27})(b_1+b_2+b_3)^2(\alpha-\alpha_r)^3 \\ & + K_1^2 b_{28}(M-M_r)^3 - K_1 b_{28}(b_1+b_2+b_3)(\alpha-\alpha_r)(M-M_r)^2 \\ & - K_1 b_{28}(b_1+b_2+b_3)(\alpha-\alpha_r)(M-M_r)^2 + b_{28}(b_1+b_2+b_3)^2(\alpha-\alpha_r)^2(M-M_r) \\ & - K_1 b_{29}(M-M_r)^2 + b_{29}(M-M_r)(b_1+b_2+b_3)(\alpha-\alpha_r) \end{aligned} \quad (4.168)$$

$$\begin{aligned}\frac{\partial Q_r}{\partial \gamma}\dot{\gamma} < {} & +K_2^2 b_{30}(\gamma-\gamma_r)^3 - K_2 b_{30}(b_4+b_5+b_6)(\alpha-\alpha_r)(\gamma-\gamma_r)^2 \\ & - K_2 b_{30}(\gamma-\gamma_r)^2(b_4+b_5+b_6)(\alpha-\alpha_r) + b_{30}(\gamma-\gamma_r)(b_4+b_5+b_6)^2(\alpha-\alpha_r)^2 \end{aligned} \quad (4.169)$$

$$\frac{\partial Q_r}{\partial \alpha}\dot{\alpha} < (K_3^2 - K_3 b_7)(\alpha-\alpha_r) - K_3\left[Q-Q_r\right] \quad (4.170)$$

In order to transition the terms into a group of linear functions that will make up terms in the bound matrix, some of the difference terms have been replaced by their maximum values as shown below.

$$\begin{aligned}\frac{\partial Q_r}{\partial M}\dot{M} < {} & (b_1+b_2+b_3)b_{26}15(\alpha-\alpha_r) - K_1 b_{26}(\alpha-\alpha_r)(4) \\ & + K_1^2 4(M-M_r)b_{27}(15) - K_1(4)b_{27}(b_1+b_2+b_3)15(\alpha-\alpha_r) \\ & - K_1(4)(b_{27})(b_1+b_2+b_3)15(\alpha-\alpha_r) + (b_{27})(b_1+b_2+b_3)^2 225(\alpha-\alpha_r) \\ & + K_1^2 b_{28}16(M-M_r) - K_1 b_{28}(b_1+b_2+b_3)(15)(4)(M-M_r) \\ & - K_1 b_{28}(b_1+b_2+b_3)(15)(4)(M-M_r) + b_{28}(b_1+b_2+b_3)^2(15)(\alpha-\alpha_r)(4) \\ & - K_1 b_{29}4(M-M_r) + b_{29}(4)(b_1+b_2+b_3)(\alpha-\alpha_r) \end{aligned} \quad (4.171)$$

$$\frac{\partial Q_r}{\partial \gamma}\dot{\gamma} < +K_2^2 b_{30}(225)(\gamma-\gamma_r) - K_2 b_{30}(b_4+b_5+b_6)(15)(15)(\gamma-\gamma_r)$$
$$- K_2 b_{30}(15)(\gamma-\gamma_r)(b_4+b_5+b_6)(15) + b_{30}(15)(b_4+b_5+b_6)^2(15)(\alpha-\alpha_r) \quad (4.172)$$

The final bounded term is as follows.

$$(Q-Q_r)(\dot{Q}-\dot{Q}_r) < -K_4(Q-Q_r)^2 - (Q-Q_r)\dot{Q}_r \quad (4.173)$$

The scalar $\dot{V}$ function can be organized into the following matrix form.

$$\dot{V} < \begin{bmatrix} |M-M_r| & |\gamma-\gamma_r| & |\alpha-\alpha_r| & |Q-Q_r| \end{bmatrix} \begin{bmatrix} & BOUND & \\ & & \\ & & \end{bmatrix}_{4x4} \begin{bmatrix} |M-M_r| \\ |\gamma-\gamma_r| \\ |\alpha-\alpha_r| \\ |Q-Q_r| \end{bmatrix} \quad (4.174)$$

The entries of the bound matrix are given below. Each entry that is not listed is zero.

$$\text{BOUND}(1,1) = -K_1 \tag{4.175}$$

$$\text{BOUND}(2,1) = \frac{(b_1+b_2+b_3)}{2} \tag{4.176}$$

$$\text{BOUND}(1,2) = \text{BOUND}(2,1) \tag{4.177}$$

$$\text{BOUND}(2,2) = -K_2 \tag{4.178}$$

$$\text{BOUND}(1,3) = -\frac{(b_8+b_{10})(4K_1^2 - 30K_1(b_1+b_2+b_3) - K_1 b_9)}{2(-K_1+b_{11}+b_{12}+b_{13}+b_{18})} \tag{4.179}$$

$$+ \frac{K_1^2(b_{16}-8K_2)}{32(-K_1+b_{11}+b_{12}+b_{13}+b_{18})^2} - \frac{K_1^2(b_{14}+b_{15}+b_{17})}{8(-K_1+b_{11}+b_{12}+b_{13}+b_{18})^2} \tag{4.180}$$

$$- \frac{4K_1^2(b_{14}+b_{15}+b_{17})(b_{19}+b_{20}+b_{21}+b_{22})}{2(-K_1+b_{11}+b_{12}+b_{13}+b_{18})^2} \tag{4.181}$$

$$+ \frac{15K_1(b_1+b_2+b_3)(b_{14}+b_{15}+b_{17})(b_{19}+b_{20}+b_{21}+b_{22})}{(-K_1+b_{11}+b_{12}+b_{13}+b_{18})^2} \tag{4.182}$$

$$+ \frac{8K_2(-K_1+b_{11}+b_{12}+b_{13}+b_{18})}{32(-K_1+b_{11}+b_{12}+b_{13}+b_{18})^2} \tag{4.183}$$

$$\text{BOUND}(3,1) = \text{BOUND}(1,3) \tag{4.184}$$

$$\text{BOUND}(2,3) = \frac{(b_4+b_5+b_6)}{2} - \frac{4K_1K_2 - 15K_2(b_1+b_2+b_3)}{8(-K_1+b_{11}+b_{12}+b_{13}+b_{18})} \tag{4.185}$$

$$- \frac{4K_1^2(8K_2+b_{16})(b_{19}+b_{20}+b_{21}+b_{22})}{2(-K_1+b_{11}+b_{12}+b_{13}+b_{18})^2} \tag{4.186}$$

$$+ \frac{15K_1(8K_2+b_{16})(b_{19}+b_{20}+b_{21}+b_{22})(b_1+b_2+b_3)}{2(-K_1+b_{11}+b_{12}+b_{13}+b_{18})^2} \tag{4.187}$$

$$- \frac{15(8K_2+b_{16})(b_{19}+b_{20}+b_{21}+b_{22})(b_1+b_2+b_3)}{8(-K_1+b_{11}+b_{12}+b_{13}+b_{18})^2} \tag{4.188}$$

$$+ \frac{15K_2(b_{23}+b_{24})(-K_1+b_{11}+b_{12}+b_{13}+b_{18})}{8(-K_1+b_{11}+b_{12}+b_{13}+b_{18})^2} \tag{4.189}$$

$$- \frac{15(b_4+b_5+b_6)(b_{23}+b_{24})(-K_1+b_{11}+b_{12}+b_{13}+b_{18})}{8(-K_1+b_{11}+b_{12}+b_{13}+b_{18})^2} \tag{4.190}$$

$$+ \frac{(225K_2b_{25})(-8K_2+b_{16})}{32(-K_1+b_{11}+b_{12}+b_{13}+b_{18})^2} \tag{4.191}$$

$$- \frac{(225b_{25}(b_4+b_5+b_6))(-8K_2+b_{16})}{32(-K_1+b_{11}+b_{12}+b_{13}+b_{18})^2} \tag{4.192}$$

$$+ \frac{(15K_2b_{25})(b_{14}+b_{15}+b_{17})}{8(-K_1+b_{11}+b_{12}+b_{13}+b_{18})^2} \tag{4.193}$$

$$- \frac{(15b_{25})(b_4+b_5+b_6)(b_{14}+b_{15}+b_{17})}{8(-K_1+b_{11}+b_{12}+b_{13}+b_{18})^2} \tag{4.194}$$

$$\text{BOUND}(3,2) = \text{BOUND}(2,3) \tag{4.195}$$

$$\text{BOUND}(3,3) = -K_3 + b_7 - \frac{15(b_8+b_{10})(b_1+b_2+b_3)^2 + b_9(b_1+b_2+b_3)}{2(-K_1+b_{11}+b_{12}+b_{13}+b_{18})} \tag{4.196}$$

$$- \frac{K_1(b_{16}-8K_2)(b_1+b_2+b_3)}{32(-K_1+b_{11}+b_{12}+b_{13}+b_{18})^2} + \frac{K_1(b_{14}+b_{15}+b_{17})(b_1+b_2+b_3)}{8(-K_1+b_{11}+b_{12}+b_{13}+b_{18})^2} \tag{4.197}$$

$$- \frac{15(b_1+b_2+b_3)^2(b_{14}+b_{15}+b_{17})(b_{19}+b_{20}+b_{21}+b_{22})}{2(-K_1+b_{11}+b_{12}+b_{13}+b_{18})^2} \tag{4.198}$$

$$- (b_1+b_2+b_3)15b_{26} + K_1 b_{26} + 120K_1 b_{27}(b_1+b_2+b_3) \tag{4.199}$$

$$+ 225b_{27}(b_1+b_2+b_3)^2 - 60b_{28}(b_1+b_2+b_3)^2 - 4b_{29}(b_1+b_2+b_3) \tag{4.200}$$

$$\text{BOUND}(1,4) = \frac{-60K_1^2 b_{27} - 16K_1^2 b_{28}}{2} \tag{4.201}$$

$$= +60K_1 b_{28}(b_1+b_2+b_3) + \frac{4K_1 b_{29}}{2} \tag{4.202}$$

$$\text{BOUND}(4,1) = \text{BOUND}(1,4) \tag{4.203}$$

$$\text{BOUND}(2,4) = \frac{-225K_2^2 b_{30}}{2} + 225K_2 b_{30}(b_4+b_5+b_6) \tag{4.204}$$

$$\text{BOUND}(4,2) = \text{BOUND}(2,4) \tag{4.205}$$

$$\text{BOUND}(3,4) = \frac{1}{2} - \frac{(b_1+b_2+b_3)15b_{26} + K_1 b_{26} + 120K_1 b_{27}(b_1+b_2+b_3)}{2} \tag{4.206}$$

$$+ \frac{225b_{27}(b_1+b_2+b_3)^2 - 60b_{28}(b_1+b_2+b_3)^2 - 4b_{29}(b_1+b_2+b_3)}{2} \tag{4.207}$$

$$- \frac{225b_{30}(b_4+b_5+b_6)^2}{2} - \frac{K_3^2 - K_3 b_7}{2} \tag{4.208}$$

$$\text{BOUND}(4,3) = \text{BOUND}(3,4) \tag{4.209}$$

$$\text{BOUND}(4,4) = -K_4 - K_3 \tag{4.210}$$

Controller gain values can be chosen to make the [BOUND] matrix negative definite, ensuring that $\dot{V} < 0$ and satisfying the second condition of Theorem 2. This section results

in Theorem 3.

Theorem 3 (Stability Guarantee) *Suppose the controls δ_e and ϕ are designed according to the feedback relations given using the Indirect Manifold Construction approach, and feedback gains are chosen to ensure the bound matrix given is negative semi-definite. Then for initial conditions in the operating region $(M, \gamma, \alpha, Q) \in D_M \; x \; D_\gamma \; x \; D_\alpha \; x \; D_Q$, the control uniformly and asymptotically stabilizes the non-minimum phase model and equivalently drives the states $M \rightarrow M_r$ and $\gamma \rightarrow \gamma_r$, keeping all states and control inputs bounded.*

Chapter 5

CONCLUSION

In this thesis, a nonlinear controller for an air-breathing hypersonic vehicle was developed using the Indirect Manifold Construction approach. The model used in this thesis is one of the highest fidelity models currently present in the literature. The challenges of controlling such a vehicle include the system's unstable zero-dynamics. This non-minimum phase behavior prevents the use of many standard nonlinear control techniques. The hierarchical control design used in the Indirect Manifold Construction approach allows the system's outputs to be driven to reference commands while ensuring the stability of the system's internal dynamics. The controller designed in this thesis asymptotically stabilizes the non-minimum phase model while keeping all states and control inputs bounded.

Future work in this area may include determining the controller's exact quantitative robustness to uncertainties in the aerodynamic and propulsive forces as well as imperfect state measurements. Also, a control input derivative limiter for smoother control inputs and less excitation of the system's internal states could be implemented.

BIBLIOGRAPHY

[1] Michael A. Bolender and David B. Doman. A nonlinear longitudinal dynamical model of an air-breathing hypersonic vehicle. *Journal of Spacecraft and Rockets*, 22(2):374–381, 2007.

[2] Michael A. Bolender and David B. Doman. Flight path angle dynamics of air-breathing hypersonic vehicles. In *AIAA Guidance, Navigation, and Control Conference and Exhibit*, 2006.

[3] Office of Technology Assessment U.S. Congress. *Round Trip to Orbit: Human Spaceflight Alternatives*. U.S. Government Printing Office, 1989.

[4] Elvia Thompson, Keith Henry, and Leslie Williams. Faster than a speeding bullet: Guinness recognizes nasa scramjet, June 2005.

[5] Daryl Meyer. X-51a waverider achieves history in final flight, May 2013.

[6] Frank R. Chavez and David K. Schmidt. Analytical aeroproulsive/aeroelastic hypersonic-vehicle model with dynamic analysis. *Journal of Guidance, Control, and Dynamics*, 17(6), November-December 1994.

[7] Michael A. Bolender and David B. Doman. A non-linear model for the longitudinal dynamics of a hypersonic air-breathing vehicle. *AIAA Paper*, 2005-6255.

[8] David K. Schmidt. Optimum mission performance and multivariable flight guidance for airbreathing launch vehicles. *Journal of Guidance, Control, and Dynamics*, 20(6), November-December 1997.

[9] J. Davidson, F. Lallman, J.D. McMinn, J. Martin, J. Pahle, M. Stephenson, J. Selmon, and D. Bose. Flight control laws for nasas hyper-x research vehicle. *AIAA Paper 1999-4124*, 1999.

[10] Kevin P Groves, David O. Sigthorsson, Andrea Serrani, Stephen Yurkovich, Michael A. Bolender, and David B. Doman. Reference command tracking for a linearized model of an air-breathing hypersonic vehicle. In *AIAA Guidance, Navigation, and Control Conference and Exhibit*, 2005.

[11] Haojian Xu, Maj D. Mirmirani, and Petros A. Ioannou. Adaptive sliding mode control design for a hypersonic flight vehicle. *Journal of Guidance, Control, and Dynamics*, 27(5), September-October 2004.

[12] Christopher I. Marrison and Robert F. Stengel. Design of robust control systems for a hypersonic aircraft. *Journal of Guidance, Control, and Dynamics*, 21(1), January-February 1998.

[13] Jason T. Parker, Andrea Serrani, Stephen Yurkovich, Michael A. Bolender, and David B. Doman. Control-oriented modeling of an air-breathing hypersonic vehicle. *Journal of Guidance, Control, and Dynamics*, 30(3):856–869, May-June 2007.

[14] Lisa Fiorentini. *Nonlinear Adaptive Controller Design For Air-Breathing Hypersonic Vehicles*. PhD thesis, The Ohio State University, 2010.

[15] Anshu Narang-Siddarth and John Valasek. *Nonlinear Time Scale Systems in Standard and Nonstandard Forms*. Society for Industrial and Applied Mathematics, 2014.

[16] Frank L. Lewis, Draguna L. Vrable, and Vassilis L. Syrmos. *Optimal Control*. John Wiley & Sons, Inc., 2012.

[17] Anshu Narang-Siddarth, Florian Peter, Florian Holzapfel, and John Valasek. Autopilot for a nonlinear non-minimum phase tail-controlled missile. In *AIAA Guidance, Navigation, and Control Conference*, 2014.

[18] Jean-Jacques E. Slotine and Weiping Li. *Applied Nonlinear Control*. Prentice-Hall, Inc., 1991.

[19] Hassan K. Khalil. *Nonlinear Systems*. Macmillan Publishing Company, 1992.

[20] Trevor Williams, Michael A. Bolender, David B. Doman, and Oscar Morataya. An aerothermal flexible mode analysis of a hypersonic vehcle. *AIAA Paper*, 2006-6647.